

2007-2010

China National Report on Seismology and Physics of the Earth's Interior

For

The 25th General Assembly of IUGG

Melbourne, Australia, 28 June - 7 July 2011

Prepared by China National Committee for International
Association of Seismology and Physics of the Earth's
Interior (IASPEI)

Contents

1. Chen Yuntai, Zhang Yong, Introduction on the recent earthquake source kinematics study in China.
2. Wang Chunyong, et al., Evidence for Mechanically Coupled Lithosphere in central Asia and resulting implications.
3. Chen Yongshun John, Progress in seismotectonic studies at Peking University.
4. Chang Lijun, Wang Chunyong and Ding Zhifeng, Seismic anisotropy of upper mantle in Sichuan and adjacent regions.
5. Fang Lihua, et al., Crustal velocity structures beneath North-China revealed by ambient noise tomography.
6. Chang Lijun, et al., Upper mantle anisotropy beneath the North China from shear-wave splitting measurements.

Introduction on the recent earthquake

source kinematics study in China

Chen Yun-Tai, Zhang Yong

Institute of Geophysics, China Earthquake Administration. Beijing 100081, China

1. Methods development

Seismologists in China pay much attention to the source kinematics problem, and have developed kinds of techniques to better understand the earthquake source physics in recent 15 years. Chen and Xu (1995) first studied on the rupture process inversion by retrieving and analyzing the ASTF (apparent source time function). Then, Yao and Ji (1997) developed a nonlinear method to investigate the rupture process of moderate-to large earthquakes. Zhou and Chen (2002) designed a linear and nonlinear iteration process to invert the near-field strong motion data for the rupture process. Zhang et al., (2008) summarized and improved several inversion methods and successfully applied them to large earthquakes.

These studies lay the foundation for further researches on earthquake rupture process. There are mainly two aspects. The first is the joint inversion study of seismic data and geodetic data (GPS data and InSAR data), since the joint analysis of kinds of datasets can constrain the complex rupture behaviors much better than single datasets and helps to image the real rupture propagations. For example, Wang et al., (2008) jointly used teleseismic data and GPS data and obtained the rupture process of 2008 Wenchuan earthquake. And the second, is the fast and routine rupture process inversion, since it can offer valuable suggestions for earthquake emergency response, such as earthquake relief and disaster estimation. For example, Chen and Zhang (2010) have made a routine work to fast determine and release the rupture process results of large earthquake.

2. Study on application of rupture process inversion to large earthquakes

As the earthquake competent department in China, in recent years, CEA (China Earthquake Administration) had realized that the source information took an important part in earthquake relief and hazards assessment, and had constructed a response system for earthquake emergency to well utilize the source information for earthquake emergency. As an important part of source information, earthquake source rupture process attracts much attention of CEA. Thus, once the large earthquake happens, a fast and robust rupture process result is highly demanded by CEA to quickly estimate the intensities and casualty losses in the epicentral area.

After the 2008 Wenchuan earthquake, the group directed by Yun-Tai Chen prepared

for several months, and then started performing the fast inversion of rupture process since January 2009. They tried best to release the fast inversion results within 5 hours after the earthquake occurrence for the earthquakes with magnitudes larger than 6.5 in China and large than 7.5 in other places in the world. Based on the former study on the ASTF and seismic wave inversion, Chen and Zhang (2010) retrieve ASTF and invert seismic waves simultaneously to get a more reliable result by using the ASTF and inversion results verify each other. This technique is so stable and robust that the group successfully obtain the rupture process results of 18 large earthquakes since January 2009 (Figure 1), and most of the inversions cost about 3~5 hours (Figure 2).

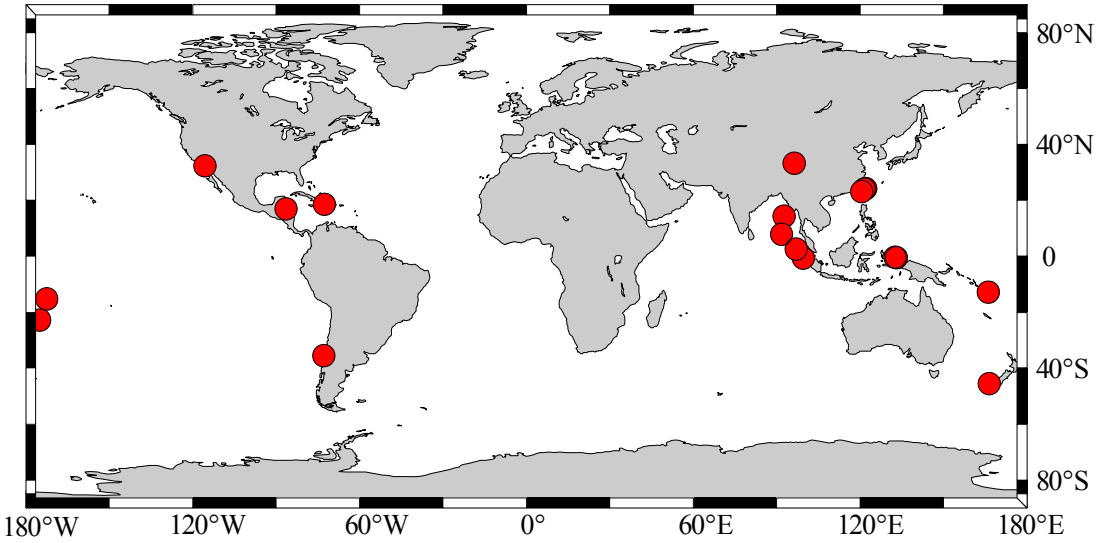


Figure 1. Epicentral location of 18 large earthquakes occurred since the January 2009.

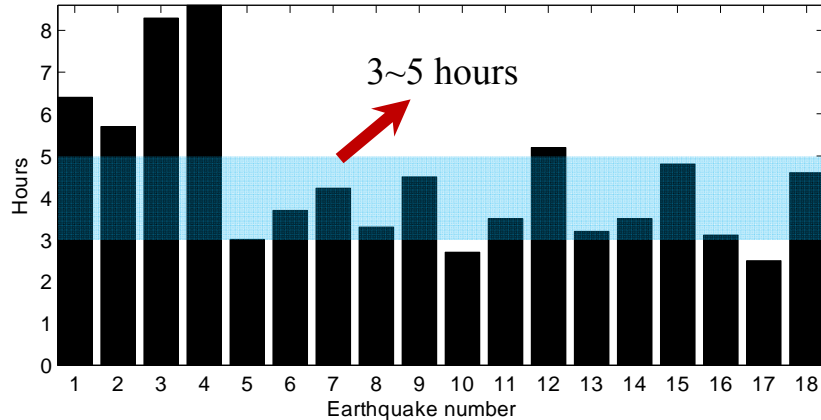


Figure 2. Time the inversion of 18 large earthquakes cost.

3. Two Recent Disastrous Earthquakes in China

In the past ten years of the 21st century, two disastrous earthquakes struck China and caused tens of thousands of death. The fist is the 12 May 2008 Wenchuan $M_w7.9$ earthquake. The Wenchuan earthquake, locating on the Longmenshan fault, the boundary of the Qinghai-Tibet Plateau and Sichuan basin, is the largest disastrous

earthquake after the 1976 Tangshan earthquake in China and caused about 86 815 death or missing. After the occurrence of the Wenchuan earthquake, seismologists in China performed analysis on the source characteristics immediately. The group directed by professor Yun-Tai Chen (2008) fast determined the source mechanism of Wenchuan earthquake sequence and the rupture process of the mainshock by using of teleseismic data, then released the results to CEA officials on the next day. In their results, two slip-concentrated patches are found to locate near Yingxiuzhen and Beichuan city, which is confirmed in most of following researches. Besides, Wang et al. (2008) also make fast investigation on the rupture behaviors of this earthquake, and found the rupture mainly propagated towards NE and the ruptured fault length is about 216 km. These primary studies offered valuable information for the earthquake relief, disaster estimation and other government decisions.

About two years later, another earthquake, the 14 April 2010 Yushu earthquake occurred in Yushu county, Qinghai province, and caused about 3000 people dead or missing. The epicentral location of this earthquake, as determined and released by CENC (China Earthquake Networks Center), is about 44 km northwest to the Yushu city. However, rupture process result (Zhang et al., 2010) obtained about 2.5 hours, 5 hours and 2 days after the earthquake occurrence consistently show that the earthquake rupture unilaterally propagates toward SE and causes a large slip-concentrated patch near the Yushu city. It suggests that the Yushu city, locating 44 km to the southeast of the epicenter, will be destroyed terribly, and should be a key area for the earthquake relief.

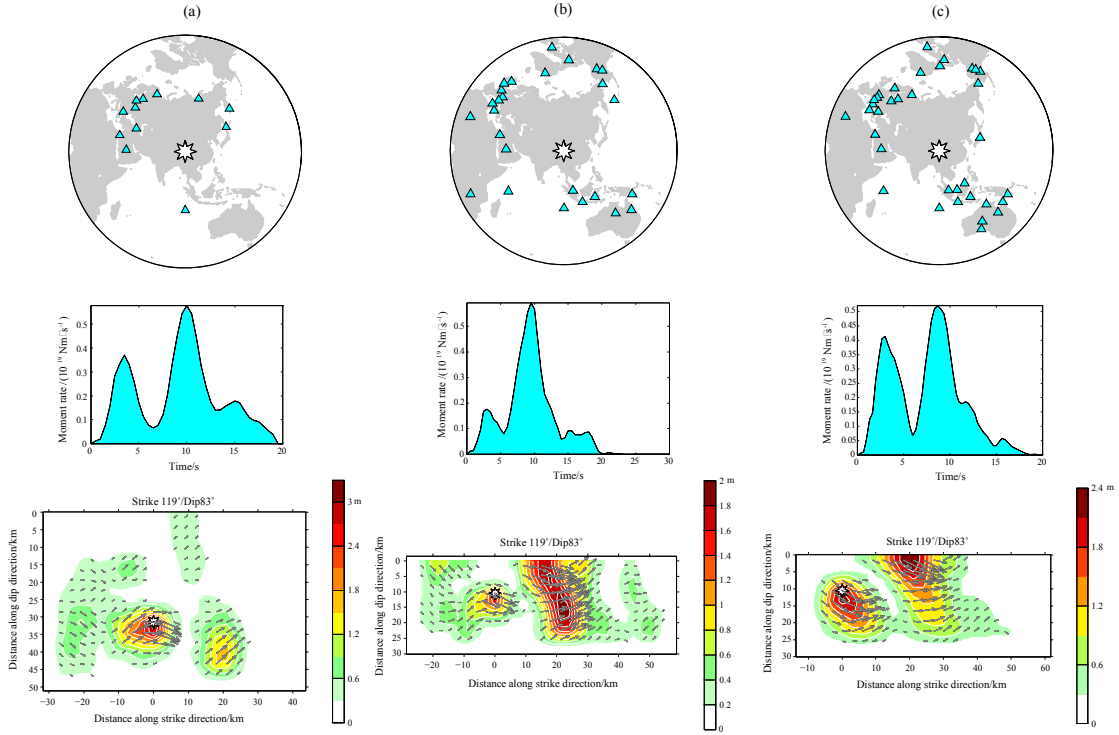


Figure 3. Fast rupture process results of 2010 Yushu, Qinghai, earthquake.

(a) obtained 2.5 hours after the earthquake occurrence; (b) obtained 5 hours after the earthquake occurrence; (c) obtained 2 days after the earthquake occurrence.

References

- Xu L S. Study on the tempo-spatial rupture process of earthquakes [Ph.D. dissertation] (in Chinese). Beijing: Institute of Geophysics, China Earthquake Administration, 1995
- Chen Y T, Xu L S. A time-domain inversion technique for the tempo-spatial distribution of slip on a finite fault plane with applications to recent large earthquakes in the Tibetan Plateau. *Geophys. J. Int.* 2000, 143:407~416
- Yao Z X, Ji C. The inverse problem of finite fault study in time domain (in Chinese). *Chinese J. Geophys.*, 1997, 140(5): 691~701
- Zhou S Y, Chen X F. Inversion of near-field waveform data for earthquake source rupture process (I): Method and numerical test. *Science in China Series D: Earth Sciences*, 2003, 46 (11): 1089 ~ 1102
- Zhang Y. Study on the inversion methods of source rupture process [Ph.D. dissertation] (in Chinese). Beijing: School of Earth and Space Science, Peking University, 2008. 1~158
- Wang W M, Yao Z X. Rupture process of the Ms 8.0 wenchuan earthquake of Sichuan, China. *Chinese J. Geophys. (in Chinese)*, 2008, 51(5): 1403~1410
- Chen Y T, Zhang Y. Fast and robust inversion of earthquake source rupture process with applications to earthquake emergency response. American Geophysical Union, Fall Meeting 2010, abstract #S43A-2044
- Chen Y T, Xu L S, Zhang Y et al., Reports on the source characters of Wenchuan great earthquake occurred on 12th May 2008 (in Chinese). China seismic information network, 2008 .<http://www.csi.ac.cn/sichuan/index080512.htm>
- Wang W M, Yao Z X. Source process of the May 12, 2008, Wenchuan Ms8.0 earthquake. http://www.csi.ac.cn/sichuan/sichuan080512_cs2.htm
- Zhang Y, Xu L S, Chen Y T. Fast inversion of rupture process of the 14 April 2010 Yushu, Qinghai, earthquake. *Earthquake Science*, 2010, 23(3):201~204

Evidence for Mechanically Coupled Lithosphere in central Asia and resulting implications

Chun-Yong Wang¹, Lucy M. Flesch², Paul G. Silver³, Li-Jun Chang¹ and Winston W. Chan⁴

1 Institute of Geophysics, China Earthquakes Administration, Beijing 100081, PR China

2 Department of Earth & Atmospheric Sciences, Purdue University, West Lafayette, Indiana 47907, USA

3 Carnegie Institute of Washington, Washington, DC20015, USA

4 Multimax Corporation, 1441 McCormick Drive, Landover, Maryland 20774, USA

Abstract

The recent dramatic increase in seismic anisotropy and surface global positioning system (GPS) data for central Asia permits a comprehensive examination of the mantle's role in mountain building. A joint analysis of 178 shear-wave-splitting and ~2000 GPS observations using a new technique reveals that the crust and lithospheric mantle deform coherently, arguing for crust-mantle mechanical coupling during deformation. The observed spatial variations in anisotropy reflect the large-scale pattern of lithospheric deformation, as well as a change in deformational style from simple shear on the Tibetan Plateau transitioning to pure shear in surrounding regions.

Keywords: anisotropy, lithospheric deformation, global positioning system, central Asia.

1. Introduction

How mountains form is one of Earth science's basic questions. Progress has been made in understanding crustal properties of continental lithosphere in the mountain-building process, i.e., the anomalous thickness and high topography created by the process of continent-continent collision. The role of the lithospheric mantle in orogeny, however, is less clear, as reflected in the range of mantle properties found in current models for orogenic deformation (England and Houseman, 1986, 1989; Royden et al., 1997; Tapponnier et al., 1982; Thatcher, 2006; Meade, 2007). If the lithospheric mantle deformation could be measured directly and compared to the surface, it would constitute an important means of assessing the mantle's role in orogens. Such a means is now available through the joint analysis of surface deformation data and mantle seismic anisotropy (Flesch et al., 2005). A recent increase in the number of both types of data in central

Asia and conceptual advances in their joint analysis provide strong support for mechanically coupled orogenic lithosphere throughout this region.

2. Geophysical Data

Mantle anisotropy is constrained with 178 SKS shear-wave splitting observations, 73 from previously published studies (McNamara et al., 1994; Huang et al., 2000; Flesch et al., 2005; Lev et al., 2006; Sol et al., 2007) and 105 new ones analyzed in this study obtained from portable deployments in Yunnan (2002) (Chang et al., 2006), eastern Tibet and Sichuan (2004-2006, China Earthquake Administration, Carnegie Institute of Washington, Saint Louis University, Multimax Corporation), and permanent stations from Chinese regional and national networks (Zhao et al., 1997) (Fig. 1). We have used standard methods (Silver and Chan, 1991; Wolfe and Silver, 1998) to calculate individual splitting observations of the fast polarization direction, ϕ , and delay time, δt , as well as station stacks. For our own observations, only those stations where splitting could unambiguously be detected were used. We proceed assuming that the seismic anisotropy arises from a single homogenous mantle layer because: (1) we checked our data for evidence of two anisotropic layers by the analysis of back-azimuthal variations in both ϕ and δt (Silver and Savage, 1994), but found none (Figs. DR1-DR3; see footnote 1) and (2) several studies have concluded that the crust cannot account for SKS splitting observations in central Asia based on studies of crustal splitting (McNamara et al., 1994; Herquel et al., 1995; Sherrington et al., 2004; Frederiksen et al., 2003; Ozcar and Zandt, 2004; Karalliyadda et al., 2007).

For the surface deformation field, we have used ~2000 global positioning system (GPS) observations (Abdrakhamatov et al., 1996; Bendick et al., 2000; Calais et al., 1998; Chen et al., 2000; Heki et al., 1999; Michel et al., 2001; Shen et al., 2000, 2001; Simous et al., 1999; Wang et al., 2001; Yu et al., 1999; Zhang et al., 2004; Zhu et al., 2000; <http://sideshow.jpl.nasa.gov/mbh/series.html>) and Quaternary fault slip rates (England and Molnar, 1997) to quantify the velocity, V_c , velocity gradient tensor, \mathbf{L}_c , and strain-rate tensor, $\boldsymbol{\epsilon}Y_c$, following the method of Haines and Holt (1993) and Haines et al. (1998) (Fig. DR4).

3. Joint Analysis of Shear-Wave Splitting

We directly compared mantle anisotropy with predicted fast polarization directions, ϕ_c , from the surface deformation field. We assume A-type lattice preferred orientation (LPO) in olivine, where the olivine a -axis is parallel to the finite-strain maximum shear direction for simple shear (Zhang and Karato, 1995), and the finite-strain extension direction for pure shear (Nicolas et al., 1973). For the nearly vertically propagating shear waves we are using, and assuming that the a -axis concentration is subhorizontal, ϕ_c will have the same orientation as the a -axis concentration. While other LPO types have been proposed for elevated stress and water content (Jung and Karato, 2001), the most successful LPO type for modeling mantle anisotropy (Davis et al., 1997; Holt,

2000; Silver and Holt, 2002; Flesch et al., 2005), and the most prevalent type found in natural mantle samples (Silver et al., 1999; Mainprice et al., 2000; Ben-Ismail et al., 2001) is A-type.

To predict the mantle finite-strain field $\boldsymbol{\epsilon}_m$ that determines the LPO from the surface instantaneous quantities \mathbf{L}_c and $\boldsymbol{\epsilon}_c$, we assume that $\boldsymbol{\epsilon}_m$ is formed by the integration of $\boldsymbol{\epsilon}_c$, over time (Kaminski and Ribe, 2002). This correspondence is straightforward under the idealized conditions of both simple and pure shear because the instantaneous and finite-strain maximum-shear and maximum-extension directions are invariant under simple shear and pure shear, respectively. Therefore, ϕ_c will be parallel to the surface-strain instantaneous maximum-shear and/or maximum-extension in a simple-shear and/or pure-shear regime. Knowledge of the continuous strain-rate field, $\boldsymbol{\epsilon}_c$, thus allows the prediction of ϕ_{ssl} , ϕ_{ssr} , and ϕ_{ps} , for left-lateral simple shear, right-lateral simple shear, and pure shear, respectively, at each splitting observation. In principle, we can use \mathbf{L}_c to determine which of these three is the correct direction by calculating the kinematic vorticity number W_k (McKenzie, 1979; Means, 1990; Fossen and Tikoff, 1993), which is a ratio of rotation to shear. Thus, W_k is ± 1 for left- and/or right-lateral simple shear and $W_k = 0$ for pure shear (Kaminski and Ribe, 2002). Values of $W_k = 0.5$ tend to result in simple shear (McKenzie, 1979). If there is external rigid-body rotation unrelated to the internal deformation generating the anisotropy, W_k will not reflect the style of internal deformation. We therefore estimate the amount of external rotation using the line rotation method (Lamb, 1987; Holt and Haines, 1993), assuming that the observed splitting orientation constitutes a deformational invariant direction (i.e., is not rotated by the internal deformation). The calculated external rotation is then removed from \mathbf{L}_c to calculate a corrected W_k^* , which is then used to choose ϕ_c (Table DR2).

We compared data in central and northern Tibet (above the Bangong-Nujiang suture) and surrounding off-plateau regions. Observations south of the Bangong-Nujiang suture are plotted but not compared because of the likely influence of Indian lithosphere (e.g., Kosarev et al., 1999). The pattern of splitting fast polarization directions exhibits several basic features (Figs. 1 and 2). There is an overall west-to-east rotation of ϕ from NE-SW to E-W, to NW-SE, to N-S. The N-S trend then abruptly rotates to E-W below $\sim 27^\circ\text{N}$ (Lev et al., 2006; Sol et al., 2007). Comparing splitting observations and predictions based on W_k^* reveals a close correspondence. Over most of the Tibetan plateau, ϕ is well predicted by $\phi_c = \phi_{ssl}$ (Flesch et al., 2005). Along the boundaries of the plateau to the southeast, northeast, and surrounding regions, it is $\phi_c = \phi_{ps}$ that successfully predicts ϕ , including the change in splitting orientations at 27°N and the more subtle west to east, WNW-ESE to ENE-WSW rotation in south of 27°N . The zone between 28°N and 30°N appears to represent a more complex transition between left-lateral simple shear and pure shear styles of deformation. Thus there appear to be two transitions: (1) from simple shear on the Tibetan plateau to pure shear along the boundaries and surrounding regions, and (2) within the pure shear regime a change from north-south to east-west splitting and extension directions (Fig. DR4). Splitting observations close to the Xianshuihe-Xiaojiang fault systems are parallel to the fault and produce

W_k^*-1 , indicating that this well-developed left-lateral fault has a strong local influence through Tibet, Sichuan, and Yunnan. Likewise, splitting observations to the east of the right-lateral Red River fault produce a W_k^*-1 . Throughout the study area there is a correlation between the predicted ϕ_c and ϕ with an average misfit of 16.7° , indicating that deformation in the lithosphere is undergoing vertically coherent deformation (Silver, 1996). Of the 178 splitting observations, there are 14 outliers with misfits larger than 70° . Examination of these stations suggests that there are additional complexities present that are not adequately being taken into account (see the Data Repository). Exclusion of these outliers reduces the misfit to 11.8° , further strengthening the argument for vertically coherent deformation.

The previously limited splitting data, while consistent with vertically coherent deformation in Tibet (Silver, 1996; Davis et al., 1997; Flesch et al., 2005), was thought to reflect a transition to crust-mantle decoupling in Yunnan (Flesch et al., 2005; Lev et al., 2006; Sol et al., 2007). The increase in splitting observations strengthens the case for vertically coherent deformation in Tibet, and argues for this same property within the surrounding regions. A hybrid model (coupling in Tibet, decoupling in Yunnan; Flesch et al., 2005) simply cannot account for the abrupt spatial transition in splitting observations between 28°N and 26°N from N-S to E-W, and produces an overall misfit of 27.4° . This transition is also observed in the extension axes of the surface strain-rate field, as well as in the orientation of the T-axes of regional crustal seismicity (Wu et al., 2004; Figs DR4b and DR5), demonstrating that it is both a crustal and mantle feature, consistent with vertically coherent deformation. This transition is expected in areas of large gravitational potential energy variations, reflecting the change from topographic gradient-parallel extension at high elevations to topographic gradient-parallel shortening at lower elevations as the collapsing lithosphere encounters resistance from surrounding medium (Flesch et al., 2001; Lev et al., 2006).

4. Discussion and Conclusions

The observed vertically coherent deformation permits us to infer that the crust and lithospheric mantle are mechanically coupled. This is because deviatoric stresses associated with gravitational potential energy variations constitute half of the stress driving deformation in central Asia (collisional boundary conditions provide the other half) (Flesch et al., 2001). Because gravitational potential energy variations reside almost solely in the crust, vertically coherent deformation requires that the resulting vertical normal stresses be transmitted into the mantle by crust-mantle mechanical coupling. Attempts to model the observed mantle anisotropy with boundary conditions alone have been unsuccessful (Flesch et al., 2005).

This result forms an observational foundation with which to assess the mantle's role in the orogenic process. For example, block models (Tapponnier et al., 1982; Thatcher, 2006; Meade, 2007) produce highly localized shear along block boundaries and broad mantle deformation beneath the blocks. Because only the latter will generate mantle anisotropy, these models are mechanically equivalent to simple asthenospheric flow (Silver, 1996) for blocks that extend into

the mantle (Lave et al., 1996), and may be assessed by solving for a best-fitting subasthenospheric mantle velocity (Silver and Holt, 2002; Flesch et al., 2005). Such a model produces a larger misfit, 27.3, than vertically coherent deformation. Thus, these “blocks” are more likely upper crustal manifestations of distributed lithospheric deformation at depth (England and Molnar, 1990).

Channelized flow in a lower crustal low-viscosity (several orders of magnitude) channel (Royden et al., 1997) decouples the crust and mantle, prohibits the transmission of vertical stresses into the mantle, and does not generate vertically coherent deformation. To maintain vertically coherent deformation, this viscosity contrast must be less than one order of magnitude and will not channelized flow (Bendick and Flesch, 2007). The convective-instability hypothesis (England and Houseman, 1989; Molnar et al., 1998) predicts the presence of an asthenospheric flow field induced by lithospheric removal. This flow, however, is unlikely to look like vertically coherent deformation.

A joint analysis of SKS splitting and surface deformation data in central Asia argues for crust and lithospheric mantle that deform coherently and are mechanically coupled, implying that the orogenic mantle survives the mountain-building process. This simple style of lithospheric deformation provides a fundamental constraint for future orogenic models.

Acknowledgements

We thank P. Burkett and W. Jiao for valuable assistance in the seismic field deployments. This manuscript benefited from discussions with M. Behn, W. Holt, D. Weeraratne, B. Savage, W. Thatcher, and the friends of Tibet discussion group. This research was conducted under support from the Continental Dynamics Program of the State Natural Scientific Foundation of China (grant 40334041) and the international Cooperation program of the Ministry of Science and Technology of China (grant 2003DF000011), Multimax Corporation, National Science Foundation grant EAR-0215616 (Silver), and the Carnegie Institution of Washington.

References:

- Abdrakmatov, K.Y., Aldazhanov, S.A., Hager, B.H., et al., 1996, Relatively recent construction of the Tien Shan inferred from GPS measurements of present-day crustal deformation rates, *Nature*, 384, 450–453.
- Bendick, R., and Flesch, L.M., 2007, Reconciling lithospheric deformation and lower crustal flow beneath central Tibet, *Geology*, 35, 895–898.
- Bendick, R., Bilham, R., Freymueller, J., et al., 2000, Geodetic evidence for a low slip rate in the Altyn Tagh fault system, *Nature*, 404, 69–72.
- Ben-Ismail, W., Barruol, G., Mainprice, D., 2001, The Kaapvaal craton seismic anisotropy: A petrophysical analysis of upper mantle kimberlite nodules, *Geophys. Res. Lett.*, 28, 2497–2500.
- Calais, E., Lesne, O., Deverchere, J., et al., 1998, Crustal deformation in the Baikal rift from GPS

- measurements, *Geophys. Res. Lett.*, 25, 4003–4006.
- Chang, L.J., Wang, C.-Y., and Ding, Z.F., 2006, A study on SKS splitting beneath the Yunnan region, *Chin. J. Geophys.*, 49, 197–204.
- Chen, Z., Burchfiel, B. C., Liu, Y., et al., 2000. Global positioning system measurements from eastern Tibet and their implications for India/Eurasia intercontinental deformation, *J. Geophys. Res.*, 105, 16,215–16,227.
- Davis, P., England, P., and Houseman, G.A., 1997, Comparison of shear wave splitting and finite strain from the India-Asia collision zone, *J. Geophys. Res.*, 102: 27511–27522
- England, P.C., and Houseman, G.A., 1986, Finite strain calculations of continental deformation; 2, Comparison with the India-Asia collision zone, *J. Geophys. Res.*, 91, 3664–3676.
- England, P.C., and Houseman, G.A., 1989, Extension during continental convergence, with application to the Tibetan Plateau, *J. Geophys. Res.* 94, 17561–17579.
- England, P. C., and Molnar, P., 1990, Right-lateral shear and rotation as the explanation for strike-slip faulting in eastern Tibet. *Nature*, 344, 140–142
- England, P.C., and Molnar, P., 1997, The field of crustal velocity in Asia calculated from Quaternary rates of slip on faults, *Geophys. J. Int.*, 130, 551–582.
- Flesch, L.M., Haines, A.J., and Holt, W.E., 2001, Dynamics of the India–Eurasia collision zone, *J. Geophys. Res.*, 106, 16435–416460.
- Flesch, L. M., Holt, W. E., Silver, P. G., Stephenson, M., Wang, C.-Y., and Chan, W. W., 2005, Constraining the extent of crust-mantle coupling in central Asia using GPS, geologic, and shear-wave splitting data, *Earth Planet. Sci. Lett.*, 238, 248–268
- Fossen, H., and Tikoff, B., 1993, The deformation matrix for simultaneous simple shearing, pure shearing, and volume changes, and its application to transpression/ transtension tectonics, *J. Struct. Geol.*, 15, 413–422.
- Frederiksen, A.W., Folsom, H., and Zandt, G., 2003, Neighbourhood inversion of teleseismic Ps conversions for anisotropy and layer dip, *Geophys. J. Int.*, 155, 200–212.
- Haines, A.J., and Holt, W.E., 1993, Procedure for obtaining the complete horizontal motions within zones of distributed deformation from the inversion of strain-rate data, *J. Geophys. Res.*, 98, 12057–12082.
- Haines, A.J., Jackson, J.A., Holt, W.E., et al., 1998, Representing distributed deformation by continuous velocity fields, *Science Report*, 98(5), 1–121, Institute of Geological and Nuclear Sciences, Wellington, New Zealand.
- Herquel, G., Wittlinger, G., and Guilbert, J., 1995, Anisotropy and crustal thickness of northern Tibet: New constraints for tectonic modeling, *Geophys. Res. Lett.*, 22, 1925–1928.
- Holt, W.E., and Haines, A.J., 1993, Velocity fields in deforming Asia from the inversion of earthquake-released strains. *Tectonics*, 12: 1–20.
- Holt, W. E., 2000, Correlated crust and mantle strain fields in Tibet, *Geology*, 28: 67–70
- Huang, W. C., Ni, J. F., Tilmann, F., et al., 2000, Seismic polarization anisotropy beneath the

- central Tibetan Plateau, *J. Geophys. Res.*, 105, 27979–27989.
- Jung, H., and Karato, S. I., 2001, Water-induced fabric transitions in olivine, *Science*, 293, 1460–1463.
- Kaminski, E., and Ribe, N., 2002, Timescales for the evolution of seismic anisotropy in mantle flow, *Geochem. Geophys. Geosyst.*, 3(1), 10.1029/2001GC000222.
- Kosarev, G., Kind, R., Sobolev, S.V., et al., 1999, Seismic evidence for a detached Indian lithospheric mantle beneath Tibet, *Science*, 283, 1306–1309.
- Lamb, S.H., 1987, A model for tectonic rotations about a vertical axis, *Earth Planet. Sci. Lett.*, 84: 75–86.
- Lave, J., Avouac, J.P., Lacassin, R., et al. 1996, Seismic anisotropy beneath Tibet: evidence for eastward extrusion of the Tibetan lithosphere? *Earth Planet. Sci. Lett.*, 140: 83–96
- Lev, E., Long, M. D., van der Hilst, R., 2006. Seismic anisotropy in eastern Tibet from shear wave splitting reveals changes in lithospheric deformation. *Earth Planet. Sci. Lett.*, 251, 293–304. doi:10.1016/j.epsl.2006.09.018.
- Mainprice, D., Barruol, G., and Ben-Ismail, W., 2000, The anisotropy of the Earth's mantle : From single crystal to polycrystal. *in* Karato, S., eds., *Mineral Physics and Seismic Tomography: From Atomic to Global*, AGU Geophysical Monograph 117. 237–264.
- McKenzie, D. 1979. Finite deformation during fluid flow. *Geophys. J. R. astr. Soc.* 58,689–715.
- McNamara, D., Owens, T., Silver, P. G., et al. 1994, Shear-wave anisotropy beneath the Tibetan Plateau. *J. Geophys. Res.*, 99: 13655–13665
- Means, W. D. 1990. Kinematics, stress, deformation and material behaviour. *J. Struct. Geol.* 12,953–971.
- Nicolas, A., Boudier, F., and Boullier, A. M., 1973, Mechanisms of flow in naturally and experimentally deformed peridotites, *Am. J. Sci.*, 273, 853–876.
- Ozacar, A.A., and Zandt, G., 2004, Crustal seismic anisotropy in central Tibet: Implications for deformational style and flow in the crust, *Geophys. Res. Lett.*, 31: L23601, doi:10.1029/2004GL021096.
- Royden, L.H., Burchfiel, B.C., King, R. W., et al., 1997, Surface deformation and lower crustal flow in eastern Tibet, 276, 788–790.
- Savage, M. K., 1999, Seismic anisotropy and mantle deformation: What have we learned from shear wave splitting, *Rev. Geophys.*, 37(1), 69–106.
- Silver, P.G., 1996. Seismic anisotropy beneath the continents: Probing the depths of geology, Annual *Rev. Earth Planet. Sci.*, 24, 385–432.
- Silver, P.G. and Chan, W.W., 1991. Shear-wave splitting and subcontinental mantle deformation, *J. Geophys. Res.*, 96, 16429–16454.
- Silver, P. G. and Holt, W.E., 2002. The mantle flow field beneath western North America, *Science*, 295, 1054–1057.

- Silver, P.G., and Savage, M., 1994, The interpretation of shear-wave splitting parameters in the presence of two anisotropic layers, *Geophys. J. Int.*, 119, 949–963.
- Silver, P. G., Mainprice, D., Ismail, W.B., et al., 1999, Mantle structural geology, in Fei, Y., et al., eds., *Mantle Petrology: Field Observations and High Pressure Experimentation: A contribute to Francis R. (Joe) Boyd*, Chemical Society Special Publication 6, 79–103. .
- Simons, W.J.F., Ambrosius, B.A.C., Noomen, R., et al., 1999, Observing plate motion s in SE Asia: Geodetic results of the GEODYSSSEA project, *Geophys. Res. Lett.*, 26, 2081–2084.
- Sol, S., Meltzer, A., Burgmann, R. et al., 2007. Geodynamics of the southeastern Tibetan Plateau from seismic anisotropy and geodesy, *Geology*, 35(6), 563–566.
- Tapponnier, P., Peltzer, G., Dain, A. Y. L., Armijo, R., Cobbold, P., 1982. Propagating extrusion tectonics in Asia: new insights from simple experiments with plasticine. *Geology* 10, 611–616.
- Thatcher, W., 2006, Microplate model for the present-day deformation in Tibet, *J. Geophys. Res.*, 111, doi:10.1029/2005JB004244.
- Wang, Q., Zhang, P. Z., Freymuller, J. T., et al., 2001, Present-day crustal deformation in China constrained by global positional system measurements. *Science*, 294: 574–577
- Wolfe, C. J., and Silver, P. G.. 1998, Seismic anisotropy of oceanic upper mantle: Shear wave splitting methodologies and observations. *J. Geophys. Res.*, 103(B1): 749–771
- Wu, J. P., Ming, Y. H., and Wang, C.-Y., 2004, Source mechanism of small-moderate earthquakes and tectonic stress field in Yunnan Province, *Acta Seismologica Sinica*, 17, 509–517.
- Yu, S.B., Kuo, L.C., Punongbayan, R.S., et al., 1999, GPS observation of crustal deformation in the Taiwan-Luzon region, *Geophys. Res. Lett.*, 26, 923–926.
- Zhang, P.Z., Shen, Z.K., Wang, M., et al., 2004, Continuous deformation of the Tibetan Plateau from global positioning system data, *Geology*, 32, 809–812.
- Zhang, S., and Karato, S. I., 1995, Lattice preferred orientation of olivine aggregates deformed in simple shear, *Nature*, 375, 774–777.
- Zhao, K., Zhuang, C.T., and Shen, S.J., 1997, A feedback broadband seismometer applying to digital seismograph network, *Earthquake*, 17(Suppl.), 36–44 (in Chinese).
- Zhu, W.Y., Wang, X.Y., Cheng, Z.Y., et al., 2000, Crustal motion of Chinese mainland monitored by GPS. *Science in China, ser. D-Earth Science*, 43, 394–400.

Figure captions.

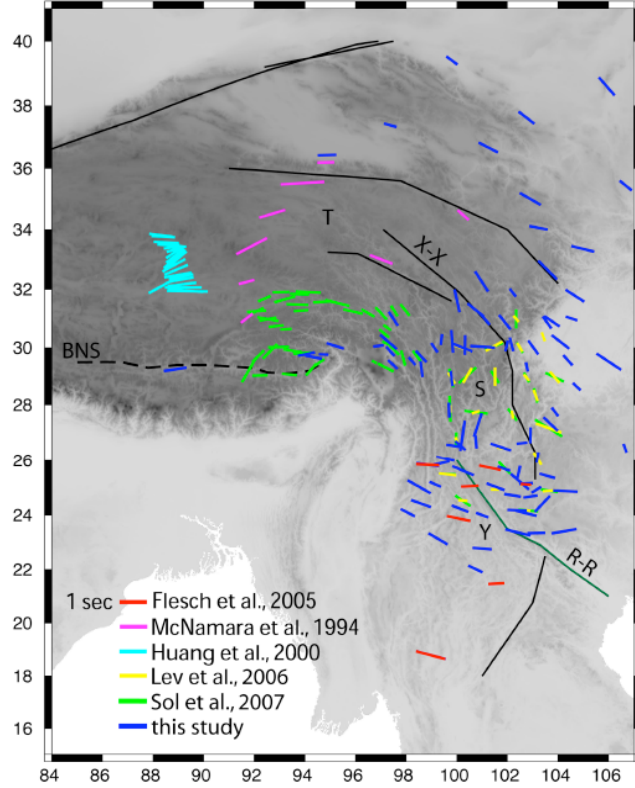


Figure 1. Shear wave splitting data set used in this study. See also Table DR1. Orientation of lines gives fast polarization direction, ϕ , and delay time, δt , given by length of bar, according to legend. These represent several previous portable deployments, one recent deployment, as well as the analysis of permanent stations from a variety of networks. Black lines represent large left-lateral faults, and green lines represent right-lateral faults. Plot is shown in degrees east and north. (X-X—Xianshuihe-Xiaojiang fault, R-R—Red Riverfault, T—Tibet, S—Sichuan, Y—Yunnan, BNS—Bangong-Nujiang suture).

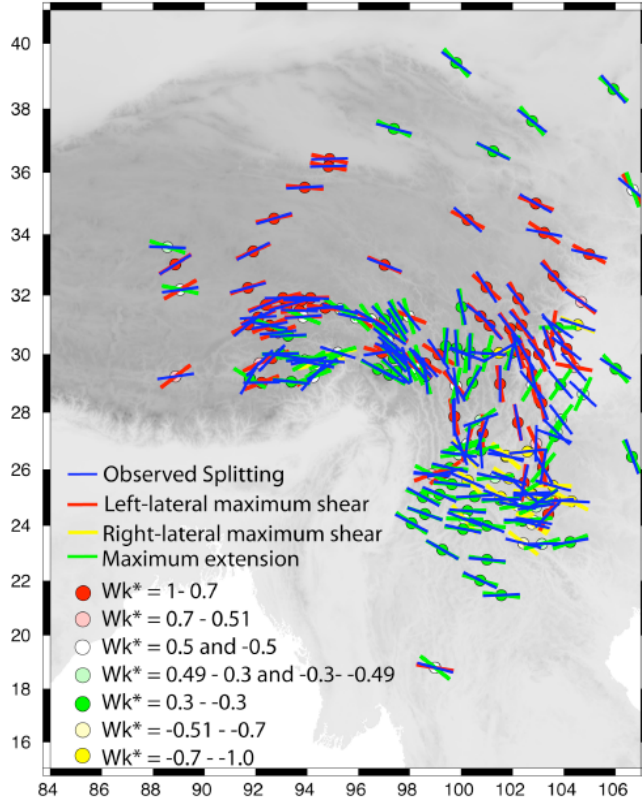


Figure 2. Comparison between predicted anisotropy direction from the surface deformation field ϕ_s , and splitting observations ϕ (observations of Huang et al. [2000] have been spatially averaged). For each observation point, we use $\phi_c = \phi_{ssi}$ (left-lateral simple shear, red), $\phi_c = \phi_{ssr}$ (right-lateral simple shear, yellow), or $\phi_c = \phi_{ps}$ (maximum extension pure shear, green), depending on value of kinematic vorticity number, W_k^* (see legend). For $W_k^* = \pm 0.5$, both pure shear and simple shear orientations are shown. Note the strong correlation between the predictions and data, as well as the systematic change in deformational style from left-lateral simple shear on the plateau to pure shear at the plateau boundaries and surrounding regions. Figure DR5 shows W_k^* plotted alone. Plot is shown in degrees east and north.

Progress in seismotectonic studies at Peking University

Yongshun John Chen

Institute of Theoretical and Applied Geophysics, School of Earth and Space Sciences, Peking University

Seismotectonics is one of the new research areas of seismology with its main focus on studying the detailed seismic structure of lithosphere and upper mantle using seismic records, particularly the records collected at portable seismic arrays. Development of new seismic methods utilizing seismic arrays such as receiver functions, SKS-splitting analysis, body- and surface-wave tomography, and recently ambient noise tomography (Langston, 1977; Dueker and Sheehan, 1997; Silver and Chan, 1991; Shapiro and Campillo, 2004) have revealed the detailed seismic structure of the world's continents and ocean basins as well. This has provided us with fundamental observations to improve our understanding of the tectonics and mantle deformation at depths at both regional and continental scales.

While networks of permanent seismic stations around the world have provided us with continued high-quality recordings, their fixed distribution in space has limited the resolution of seismic images of the continental lithosphere, particularly in regions with few permanent seismic stations or with no seismic rays passing through. Fortunately, portable seismographs which became available to seismologists since the 1980s have filled in the gap since they could be deployed at almost any place on the continents. Later they could even be deployed at seafloor as ocean bottom seismographs (OBS) with a much higher cost, of course.

Most of the portable seismographs including some of the OBSs now are broadband instruments, which enable seismologists to apply array techniques and new methods such as finite frequency tomography to significantly improve the resolution of seismic images of the lithosphere and upper mantle structures beneath the continents and part of the ocean basins (e.g., Hung et al., 2004).

The continued continental collision process between the Indian and Asian continents has built not only the world's highest mountain belt (the Himalayas) with elevations as high as 8.9 km (the Mount Everest) but also the world's largest plateau (Tibetan Plateau) with an average elevation of 5 km. The interplay between the continental collision at Tibet and the subduction process of the Pacific and Philippine Sea plates in the western Pacific controls the large-scale tectonics of the East Asia including the destruction of the North China craton.

The complex large-scale tectonics of East Asia has been the focus of seismotectonic studies for the past thirty years. Ever since the first Sino-French seismic array along the Golmod-Lhasa road in the early 1980s a number of portable seismic arrays have been deployed in Tibet and the rest of the Chinese mainland. While most of these field programs in the last century were led by western scientists and used funding from outside of China, an increasing number of field programs conducted in the past 10 years were led by Chinese scientists and funded by agencies within China. With the rapid increase in the number of portable broadband seismographs among various institutions in China, portable seismic arrays have become a regular and effective way to obtain broadband seismic records at boundaries and interiors of important tectonic units of Chinese mainland.

The progress of the seismotectonics program at Peking University is one of the examples of the rapid development in seismotectonics research at several institutions in China. Supported by the Peking University's "985" fund, the first group of 16 portable broadband seismographs imported from abroad arrived at the Institute of Theoretical and Applied Geophysics (ITAG) of the School of Earth and Space Sciences (SESS) at Peking University in December 2004. These 16 seismographs were deployed in southern Tibet in May 2005 as part of the international field program of Hi-CLIMB (Phase II). This is the first time that the faculty and students at Peking

University went out to the field and deployed their own seismographs. The success in completing the 14-month long recording in southern Tibet and the subsequent publications at international peer-reviewed journals (Fu et al., 2008; 2010; Jin et al., 2009; Jiang et al., 2009; Liang et al., 2008; 2010; Nabelek et al., 2009; Wei et al., 2010) not only officially kicked off the beginning of the seismotectonics program at Peking University but also effectively introduced the program to the international community. With continued support from the Peking University the second group of 24 broadband seismographs was imported in the summer of 2006. They were immediately deployed at the eastern boundary of Odors across the Shanxi graben.

While Peking University has only 40 portable broadband seismographs they have been effectively deployed as small seismic arrays (20 stations) at several important tectonic boundaries of China such as the seismic active fault zones around the Odors block and the northern and northeastern boundary of Tibetan Plateau. Since May 2005 the seismotectonics group at Peking University has collected more than 380 station-years of seismic records and the preliminary results have been reported at international conference such as American Geophysical Union Fall meetings (Zhou et al., 2006; Jin et al., 2006, 2008; Liang et al., 2006, 2007, 2009; Tang et al., 2006; Fu et al., 2006; Chen et al., 2007a, b, 2008; Chen and Jin, 2008; Wei et al., 2008, 2009; Wang et al., 2009; Yue et al., 2009) and national conference such as CGS annual meetings. Since 2008 the seismotectonics group at Peking University has deployed over 100 stations along an east-west linear array from Qingdao at the Sandong peninsula to the Qinghai Lake in northern Tibet. This deployment is part of the North China Craton Seismic Arrays project funded by the Chinese Natural Science Foundation's new initiative known as the "North China Craton destruction" program. The collective effort by the seismotectonics group at Peking University and groups at other institutions in China will not only provide the Earth science community the important seismic observations of the crust and upper mantle structure beneath the Chinese mainland but also will eventually put Chinese scientists to the leading position in understanding the large-scale tectonics in East Asia.

Finally, as the guest editor of the special issue of "Seismotectonics of Asia", I sincerely thank the authors of the papers included here for their contribution to the "young" scientific journal of *Earthquake Science*, which has the ambitious plan to become one of the most important journals in earthquake science in Asia. While achieving that objective will be a long and hard uphill battle the enthusiastic support and contributions from Chinese community such as this special issue is the key to shorten and finish that uphill journey. Therefore, I strongly encourage all seismologists and geophysicists to submit your valuable contributions to *Earthquake Science*, the peer-reviewed English journal in China.

References

- Dueker K and Sheehan A (1997). Mantle discontinuity structure from midpoint stacks of converted P to S waves across the Yellowstone hotspot track. *J Geophys Res* 102(B4): 8 313–8 327.
- Fu Y V, Chen Y J, Li A, Zhou S, Liang X, Ye G, Jin G, Jiang M and Ning J (2008). Indian mantle corner flow at southern Tibet revealed by shear wave splitting measurements. *Geophys Res Lett* 35: L02308, doi: 10.1029/2007GL031753.
- Fu Y, Li A and Chen Y J (2010). Crustal and upper mantle structure of Southeast Tibet from Rayleigh wave tomography. *J Geophys Res*, in press.
- Hung S-H, Shen Y and L-Y Chiao (2004). Imaging seismic velocity structure beneath the Iceland hot spot: A finite frequency approach. *J Geophys Res* 109: 08305.
- Jiang M, Zhou S, Tong X, Liang X and Chen Y J (2009). Accurate depth determination of deep earthquake in southern Tibet and its geodynamics implication. *Chinese J Geophys* 52(9): 2 237–2 244 (in Chinese).
- Jin G, Chen Y J and Basang C (2009). Investigation of local earthquakes in the Lhasa region. *Chinese J Geophys* 52(12): 3020–3026 (in Chinese).
- Langston C A (1977). Corvallis, oregon, crustal and upper mantle receiver structure from teleseismic P-waves and S-waves. *Bull Seismol Soc Am* 67(3): 713–724.
- Liang X, Zhou S, Chen Y J, Jin G, Xiao L, Liu P, Fu Y, Tang Y, Lou X and Ning J (2008). Earthquake distribution in southern Tibet and its tectonic implications. *J Geophys Res* 113: B12409, doi: 10.1029/2007JB005101.
- Liang X, Shen Y, Chen Y J and Ren Y (2010). Crustal and mantle velocity models of southern Tibet from finite frequency tomography. *J Geophys Res*, in press.

- Nabelek, J., G. Hetenyi, J. Vergne, S. Sapkota, B. Kafle, M. Jiang, H. Su, Y. J. Chen, B.-S. Huang, and the Hi-CLIMB Team (2009). Underplating in the Himalaya-Tibet collision zone revealed by the Hi-CLIMB experiment. *Science*, 325, 1371-1374, DOI: 10.1126/science.1167719.
- Shapiro N M and Campillo M (2004). Emergence of broadband Rayleigh waves from correlations of the ambient seismic noise. *Geophys Res Lett* 31(7), doi: 10.1029/2004GL019491.
- Silver P G and Chan W W (1991). Shear wave splitting and sub-continental mantle deformation. *J Geophys Res* 96: 16 429–16 454.
- Wei S, Chen Y J, Sandvol E, Zhou S, Yue H, Jin G, Hearn T M, Jiang M, Wang H, Fan W, Liu Z, Ge Z, Wang Y and Ni J (2010). Regional earthquakes in northern Tibetan Plateau: Implications for lithospheric strength in Tibet. *Geophys Res Lett* 37: L19307, doi: 10.1029/2010GL044800.
- AGU Fall Meeting Abstracts (17) of PKU Seismotectonics Group:
- Jin G, Chen Y J, Sandvol E, Zhou S-Y, Tang Y-C, Liang X-F, Ye G, Wilson D C and Nábelek J (2006). Receiver function images of the crust and upper mantle structure of southern Tibet. *Eos Trans AGU* 87(52), Fall Meet. Suppl., Abstract T53F-04.
- Liang X, Zhou S-Y, Xiao L, Jin G, Liu P, Fu Y-Y, Tang Y-C, Lou X-T, Ning J-Y, Chen Y J and Nábelek J (2006). Joint inversion for earthquake locations and 2D velocity structure beneath southern Tibet. *Eos Trans AGU* 87(52), Fall Meet. Suppl., Abstract T53F-01.
- Tang Y-C, Chen Y J, Sandvol E, Zhou S-Y, Jin G, Fu Y-Y, Liang X-F, Ning J-Y, Feng Y-G, Wang L, Liu M and Wilson D C (2006). Receiver function study of a seismic array across the western Weihe graben, the southern boundary of the Ordos. *Eos Trans AGU* 87(52), Fall Meet. Suppl., Abstract T54C-08.
- Zhou S-Y, Chen Y J, Liang X, Ye G, Jin G, Fu Y-Y, Tang Y-C, Ning J-Y and Nábelek J (2006). A temporary broadband seismic array in Southern Tibet. *Eos Trans AGU* 87(52), Fall Meet. Suppl., Abstract T53F-02.
- Chen Y J, Chen L, Zheng T and Zhou S (2007a). Integrated seismic arrays for imaging the north China Craton: the “Destruction of the North China Craton” project. *Eos Trans AGU* 88(52), Fall Meet. Suppl., Invited Abstract T22D-04.
- Chen Y J, Zhou S, Ning J, Feng Y, Tang Y, Jin G, Fu Y, Sandvol E and Liu M (2007b). Seismic array observations at the boundary of Ordos plateau, North China. *Eos Trans AGU* 88(52), Fall Meet. Suppl., Abstract T22D-05.
- Fu Y, Chen Y J, Li A, Zhou S, Ning J, Feng Y, Tang Y, Jin G, Liang X, Jiang M, Sandvol E and Liu M (2007). Strong crust-mantle coupling at Ordos plateau in North China inferred from shear-wave splitting observations of three seismic arrays at its boundary. *Eos Trans AGU* 88(52), Fall Meet. Suppl., Abstract T22D-02.
- Liang X-F, Shen Y and Chen Y J (2007). Crustal and mantle velocity models of southern Tibet from finite frequency tomography. *Eos Trans AGU* 88(52), Fall Meet. Suppl., Abstract T23F-06.
- Chen Y J and Jin G (2008). Seismic evidence for the Moho in southern Tibet as a phase change boundary. *Eos Trans AGU* 89(53), Fall Meet. Suppl., Abstract T11E-07.
- Jin G, Tang Y-C, Zhou S-Y and Chen Y J (2008). Spectra Analysis of the Wenchuan (8.0) Great Earthquake and its aftershocks. *Eos Trans AGU* 89(53), Fall Meet. Suppl., Abstract U23B-0049.
- Wei S, Jin G and John Chen Y (2008). Preliminary evidence for the presence of the Hainan plume from shear wave splitting analyses of a temporary seismic array. *Eos Trans AGU* 89(53), Fall Meet. Suppl., Abstract DI13A-1683.
- Chen Y J, Zhou S, Ning J, Tang Y, Jin G, Fu Y, Sandvol E and Liu M (2008). Seismic array observations at the boundary of Ordos plateau, North China, invited abstract, SAA 2008 meeting in Santa Fe, April 18, 2008.
- Liang X-F, Chen Y J, Sandvol E, Yue H, Hearn T and Ni J (2009). Upper mantle structure of the Eastern Tibetan Plateau from finite frequency body wave tomography. *Eos Trans AGU* 90, Fall Meet. Suppl., Abstract T14C-06.
- Tang Y, Chen Y J, Yang Y and Ding Z (2009). Ambient noise and surface wave tomography in North China. *Eos Trans AGU* 90, Fall Meet. Suppl., Abstract T11B-1806.
- Wang H, Chen Y J, Sandvol E, Zhou S, Gai Z, Feng Y, Wang Y, Yue H, Tang Y, Wei S, Fan W, Cao Y, Li P, Wang R, Hearn T and Ni J (2009). Seismic anisotropy of northern Tibet: Combine data from Indepth IV array and permanent stations. *Eos Trans AGU* 90, Fall Meet. Suppl., Abstract T11B-1803.
- Wei S, Chen Y J, Yue H, Jin G, Liang X, Zhou S, Ge Z, Feng Y, Wang Y, Tang Y, Wang H, Cao Y, Fan W, Li P, Wang R, Sandvol E, Hearn T and Ni J (2009). Indepth IV passive seismic array: Locating regional earthquakes in northern Tibet. *Eos Trans AGU* 90, Fall Meet. Suppl., Abstract T11B-1801.
- Yue H, Chen Y J, Zhou S, Feng Y, Wang Y, Ge Z, Tang Y, Wei S, Wang H, Cao Y, Li P, Liang X, Sandvol E, Hearn T and Ni J (2009). Crust and upper mantle characteristic of Northern Tibet: Receiver function and ambient noise tomography results of Indepth IV array. *Eos Trans AGU* 90, Fall Meet. Suppl., Abstract T11B-1794.

Seismic anisotropy of upper mantle in Sichuan and adjacent regions

CHANG Lijun, WANG Chunyong ^{*}, Ding Zhifeng

Institute of Geophysics, China Earthquake Administration, Beijing 100081, China

Abstract

Based on the polarization analysis of teleseismic SKS waveform data recorded at 94 broadband seismic stations in Sichuan and adjacent regions, the SKS fast-wave direction and the delay time between the fast and slow shear waves were determined at each station by use of the grid searching method of minimum tangent energy and the stacking analysis method, and the image of upper mantle anisotropy was acquired. The fast-wave polarization directions are mainly NW-SE in the study area, while it is NWW-SEE in the northeastern, and NS in the western. The delay time falls into the interval [0.47s, 1.68s]. The variation of the fast-wave directions is similar to the variation of GPS velocity directions. The anisotropic image indicates that the regional tectonic stress field has resulted in deformation and flow of upper mantle material, and make the alignment of upper mantle peridotite lattice parallel to the direction of material deformation. The crust-upper mantle deformation in Sichuan and adjacent regions accords with the mode of vertically coherent deformation. In the eastern Tibetan Plateau, the crustal material extrude to east or southeast due to SE traction force of the upper mantle material. The extrusion might be obstructed by rigid block under the Sichuan Basin and the crust has been deformed. After a long-term accumulation of tectonic strain energy, the accumulative energy suddenly released in Yingxiu town of the Longmenshan region, and Wenchuan Ms8.0 earthquake occurred.

Key words: upper mantle anisotropy, SKS wave, fast-wave polarization direction, lithospheric deformation, Wenchuan Ms8.0 earthquake.

*Corresponding author, E-mail: wangcy@cea-igp.ac.cn

Sichuan and adjacent regions are situated in the eastern Tibetan Plateau, where the tectonic setting is complicated. It belongs to three tectonic domains: the Tethyan-Himalayan tectonic domain in the west, the Pacific Ocean tectonic domain in the east, and the Paleo-Asiatic tectonic domain in the north^[1]. The study area is divided by the boundary of Beichuan-Wenchuan-Kangding-Xiaojinhe into the eastern part (the Yangtze block) and the western part (the Songpan-Garze fold system and the Sanjiang fold system). Sichuan and adjacent regions are located in the central segment of the North-South Seismic Belt, where many large earthquakes had occurred. Wenchuan Ms8.0 earthquake of May 12, 2008 has made serious injuries and deaths of the peoples and losses of property.

The Tibetan Plateau is the result of collision between the Indian and Eurasian plates, which began at about 50 Ma, and has resulted in the convergence of more than 2000 km, and the uplift of the plateau to elevation of 4–5 km^[2]. The Songpan-Garze block and the Longmenshan fault zone in the eastern margin of the Tibetan Plateau have experienced the strong crustal deformation and faulting. Recently, some papers respectively presented the evolution models of the Tibetan Plateau, i.e. the ductile flow in lower crust^[3] and the vertically coherent deformation^[4,5]. Ductile flow in the lower crust implies that the lower crust is weak, where material flows in ductile pattern. Vertically coherent deformation indicates the crust-mantle deformation is coherence, which plays a significant role in the study of evolution of the Tibetan Plateau.

Seismic anisotropy is one of the [effective methods](#) for understanding of the crust and upper mantle deformation. The anisotropy can be used to understand the intraplate deformation features, and the deformation status of lithospheric mantle related to the plate tectonic movements. The anisotropy in upper crust is mainly determined by the orientation alignment of a plenty of cracks under the action of stress, while the anisotropy in mid-lower crust is mainly determined by the lattice-preferred orientation of anisotropic mineral (such as biotite and hornblende)^[6]. Some studies concludes that the crustal anisotropic fast-wave direction is basically consistent with the strike of the active faults, and is related with the regional horizontal principal compressive stress, which is conducive to the study of crustal movement and earthquake monitoring^[7,8]. The mantle anisotropy is generally considered to be caused by the lattice-preferred orientation of olivine crystals^[9]. The plate motion is a direct cause resulting in the mantle deformation. The size and

direction of the mantle anisotropy strongly depend on the velocity and direction of the plate motion.

Many geoscientists have paid attention to the mantle deformation beneath the Tibetan plateau, and carried out a lot of relevant anisotropic studies^[10-17]. The SKS wave splitting results were obtained at some seismic stations in Sichuan and adjacent regions^[15-17], but there are no more broadband seismic stations. Since 2007, fifty-two broadband seismic stations have been deployed and operated in Sichuan, with relatively even station distribution and high data quality, which provide an advantageous condition for studying the upper mantle anisotropy. The upper mantle anisotropies, combining with the geologic, geodesy and geophysical data (GPS, crustal stress field, Quaternary fault slip rates, et al.), are used to discuss the continental dynamic issues, such as the mechanism of continental strong earthquakes, the coupling of crust and mantle.

1 Seismic Data

The observational data come from the digital records at 84 permanent broadband seismic stations and 10 temporary broadband digital seismic stations in Sichuan and adjacent regions (Table 1). The teleseismic events were collected at distance between 85° and 110° and with magnitude $M_s > 6.0$ for shallow earthquake (focal depth<150km) or $M_s > 5.5$ for deep earthquake (focal depth>150km). A total of 60 teleseismic events were collected in this study (Fig.1). Most events come from the Fiji-Tonga area in south Pacific Ocean. as a whole, the azimuthal distribution of events meets the requirements of this study.

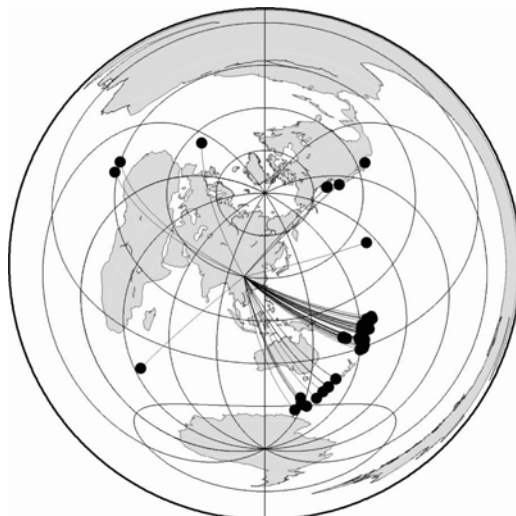


Fig.1 Epicenters of events (black dots) used in the study.

2 Analysis Method

The SKS splitting analysis method includes two steps. At first, we use the method of Silver and Chan (1991)^[9], i.e. the grid searching method of the minimum tangent energy, to make measurement of the anisotropic parameters and their error determined by individual events with different azimuths, where 95% confidence is used to the errors estimation. Then, a group of anisotropic parameters from individual events at a station are stacked by the splitting parameters method similar to that presented by Vinnik et al. (1989)^[18]. The stacking analysis is an effective method to raise the accuracy of SKS splitting measurement at a station^[19]. In this study, the splitting parameters of teleseismic SKS waves of each station were obtained by use of the stacking analysis method.

When the epicentral distances at 85°~110°, SKS wave travels along a ray path near-vertical incident on the ground. Assuming that the media are isotropic, when SKS wave penetrates the core–mantle boundary, it is radially polarized, with radial component (SV wave), and without tangent component (SH wave). When there are anisotropic layers in mantle, SKS splits into two phases with different velocities (i.e. fast and slow waves) traveling at directions orthogonal with each other, and then the particle motion changes from the originally linear polarization to elliptic polarization. The parameter pair $(\varphi, \delta t)$ is generally used to describe seismic anisotropy, where φ denotes the fast-wave polarization direction, and δt is the delay time between fast and slow waves. We can describe S wave splitting using the parameters of $(\varphi, \delta t)$, since $T(t)=0$ before the SKS wave propagates through anisotropic layer, if we can find the pair $(\varphi, \delta t)$ that they correspond with the minimum horizontal transverse component, when used to correct for anisotropy, the anisotropy parameters of station are the pair $(\varphi, \delta t)$. The method of SC is a method of measuring the anisotropic parameters $(\varphi, \delta t)$ beneath seismic stations based on the theory of the minimum tangent energy, the errors of the pair $(\varphi, \delta t)$ were determined by *F*-test, where 95% confidence was used to the error estimation. The stacking analysis, firstly, we used the method of SC to make measurement of the anisotropic parameters and their error determined by individual events with different azimuths. Then, a group of anisotropic parameters from individual teleseismic events at the station are stacked. Fig.2 shows the samples of SKS splitting analysis for Fiji earthquake (2007/10/16/21/04 with Mw6.6) at station MNI. In fig.2a, the distinct transverse component

denotes the SKS-wave splitting when it propagates through an anisotropic medium, and the particle motion become elliptical (Fig.2c). Contour plot (Fig.2e) of E_t on the corrected SKS transverse component computed through the entire range $(\varphi, \delta t)$. From Fig.2e, we can find the minimum (the star), the corresponding $(\varphi, \delta t)$ are the anisotropic results of station. The transverse component of corrected SKS phase (Fig.2b) is not distinct, the particle motion (Fig.2d) of the corrected SKS phase become linear. Hence, the S wave splitting parameters are credible.

Generally, there are N events with different back-azimuths at a station. For i th event, different parameter pair $(\varphi, \delta t)$ in the grid searching is correspondent to different tangent energy $E_t(\varphi, \delta t)_i$. Each tangent energy $E_t(\varphi, \delta t)_i$ was normalized with the minimum tangent energy, and then we summed $E_t(\varphi, \delta t)_i$ by $E_t(\varphi, \delta t) = \sum E_t(\varphi, \delta t)_i$, the minimum tangent energy of $E_t(\varphi, \delta t)$ is found by using the grid searching, and the corresponding parameter pair is the final anisotropic parameters beneath the station. The error estimation can be obtained in the similar way. For SKS waves with different azimuths and different signal-noise ratios, this method raises the reliability of the splitting result, especially for the stations with larger background noise. Fig.3 shows that the individual SKS splitting result of 2 teleseismic events (2007/08/28/12/37 with Mw6.1 and 2007/09/30/09/47 with Mw6.7), which were recorded at station GZI , are compared to the result by using the stacking analysis. It is obvious that the error of the stacked result decreases significantly, comparing with the errors of the individual events.

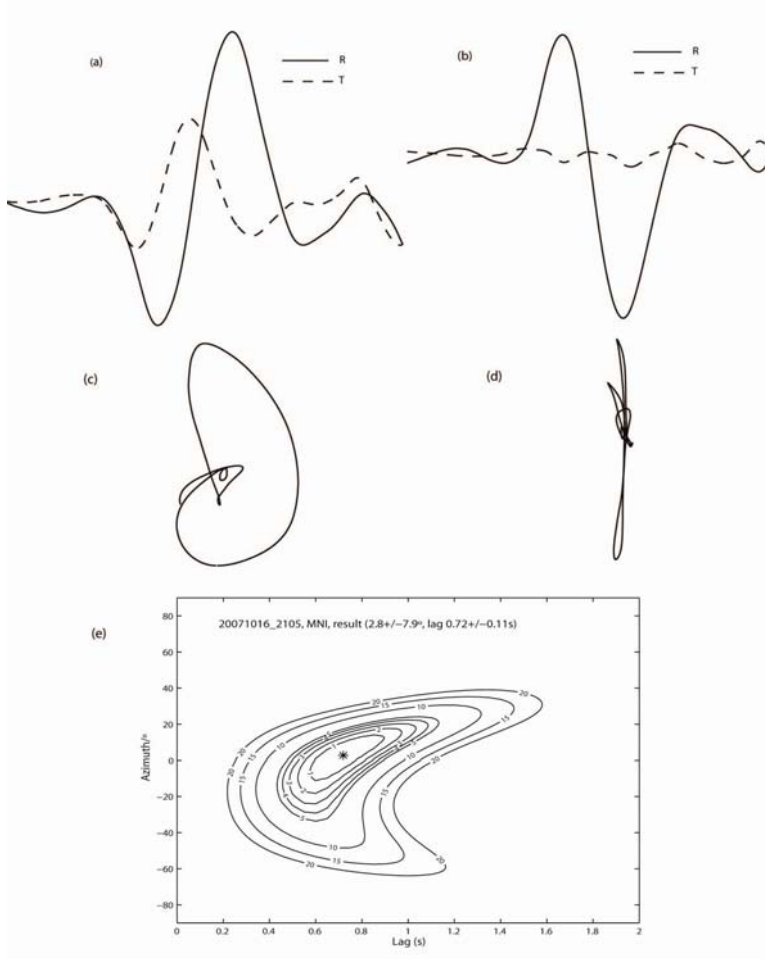


Fig. 2 An example of SKS splitting analysis

(a) Original waveform and (c) particle motion of the SKS phase in the radial-tangent coordinate system; (b) Corrected waveform and (d) particle motion of the corrected SKS phase in the radial-tangent coordinate system; (e) Contour plot of tangent energy.

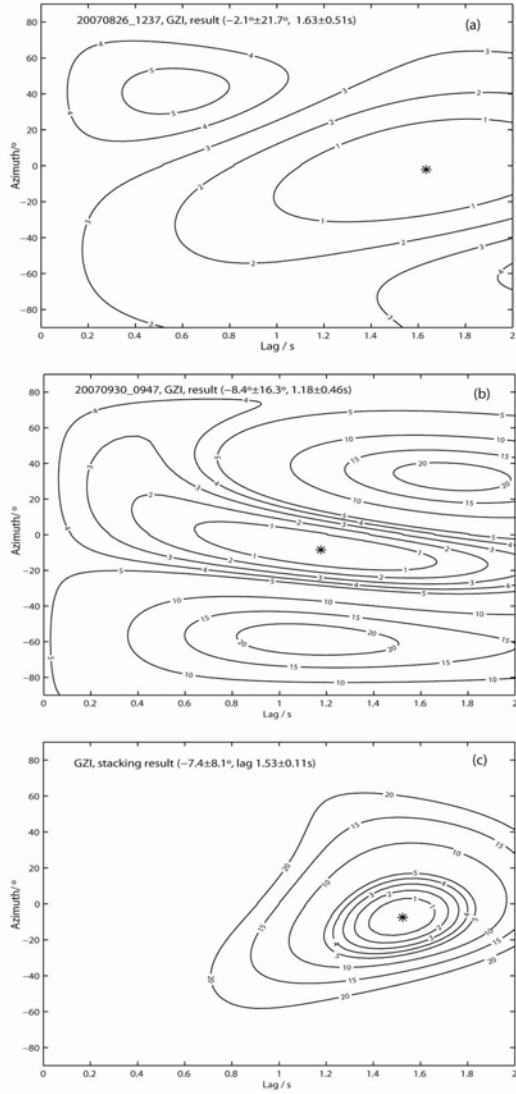


Fig.3 Tangent energy contour of SKS splitting analysis at station GZI from two teleseismic events (a) and (b), and the tangent energy contour of the result after stacking (c), where the asterisk denotes the position of optimal parameter pair.

3 Results of SKS splitting measurement and Analysis

The SKS splitting results of 94 stations in Sichuan and regions are listed in Table 1, where the splitting parameters of 52 stations were recently obtained. The results of the remainders were previously published^[14-16], but we remeasured the results at some stations which have new seismic records. In general, the permanent stations have been kept in operation for longer time under the good observational environment with low background noise, hence lots of available teleseismic events were obtained, thus SKS splitting results have high quality. In Table 1, the results of SKS

splitting measurements at most stations are good, the error of azimuth is less than 10°, and the error of delay time is less than 0.2 s. Though the adverse observational environment of the temporary stations, we have collected lots of teleseismic records available for SKS splitting analysis at those stations in the observed period of two years or so. Besides, the involvement of the stacking analysis method enables the measurements with good quality at most stations.

Based on the polarization analysis from teleseismic SKS data recorded at the 94 stations in study area, Fig. 4 shows an anisotropic image of the upper mantle. The fast-wave polarization direction is mostly NW-SE, while it is NWW-SEE in the northeastern, NW-SE in the middle, and NS in the western. However, there are some exceptions. The fast-wave directions at three stations (JCH, PZH and HLI) in the latitude 26.5°N and at two stations (LIT and YJI) in the latitude 30°N in the western of the study area are EW. The fast-wave directions at stations QCH, HZH, MAX and MIX in the east segment of the Longmenshan fault zone are NE or NEE, and the directions at stations YZP and WCH in the west segment are near NS. The delay time between fast and slow waves falls into the interval [0.47s, 1.68s], and the delay time at most stations is about 1s. In the mass, the delay time at stations located on the east of the Longmenshan fault zone is less than the delay time at stations located on the west.

Table 1 Splitting parameters for SKS phase in the study area

| No. | Code | Station | φ (°) | $\Delta\varphi$ (°) | δt (s) | $\Delta\delta t$ (s) | Num. of | Remark |
|-----|------|-----------|---------------|---------------------|----------------|----------------------|---------|--------|
| 1 | AXI | Anxian | 118.5 | 6.9 | 0.95 | 0.13 | 7 | 1 |
| 2 | BTA | Batang | 129.7 | 5.4 | 0.62 | 0.10 | 10 | 1 |
| 3 | BYD | Bingyidi | 142.9 | 4.9 | 0.57 | 0.05 | 9 | 1 |
| 4 | BZH | Bazhong | 106.7 | 6.7 | 0.90 | 0.13 | 11 | 1 |
| 5 | DFU | Daofu | 159.4 | 7.6 | 0.85 | 0.08 | 9 | 1 |
| 6 | EMS | Emeishan | 110.4 | 7.3 | 0.62 | 0.15 | 9 | 1 |
| 7 | GDS | Guodashan | 12.2 | 3.7 | 0.60 | 0.13 | 4 | 1 |
| 8 | GZA | Guza | 147.8 | 6.6 | 0.65 | 0.19 | 11 | 1 |
| 9 | GZI | Ganzi | 170.1 | 4.1 | 1.50 | 0.08 | 13 | 1 |
| 10 | HLI | Huili | 76.5 | 8. 1 | 0.57 | 0.06 | 13 | 1 |
| 11 | HMS | Huamashi | 135.1 | 6.7 | 0.87 | 0.33 | 8 | 1 |
| 12 | HSH | Heishui | 122.6 | 2.6 | 1.32 | 0.28 | 9 | 1 |

| | | | | | | | | |
|----|-----|-------------|--------|------|------|------|----|---|
| 13 | HWS | Hanwangshan | 152.2 | 6.5 | 0.58 | 0.05 | 12 | 1 |
| 14 | HYS | Hongyashan | 128.6 | 3.7 | 0.67 | 0.10 | 11 | 1 |
| 15 | JJS | Jinjisi | 115.8 | 3.0 | 0.68 | 0.12 | 9 | 1 |
| 16 | JLI | Junlian | 123.0 | 3.4 | 0.95 | 0.13 | 10 | 1 |
| 17 | JLO | Jiulong | 165.7 | 9.3 | 0.76 | 0.10 | 13 | 1 |
| 18 | JMG | Jianmenguan | 109.2 | 2.9 | 0.72 | 0.05 | 12 | 1 |
| 19 | JYA | Jingyan | 128.7 | 3.7 | 0.62 | 0.10 | 8 | 1 |
| 20 | LBO | Leibo | 160.0 | 5.1 | 0.68 | 0.05 | 11 | 1 |
| 21 | LGH | Luguhu | 43.2 | 3.7 | 1.04 | 0.21 | 9 | 1 |
| 22 | LTA | Litang | 96.9 | 5.3 | 0.94 | 0.13 | 13 | 1 |
| 23 | LZZ | Laozhaizi | 123.8 | 1.1 | 1.41 | 0.25 | 5 | 1 |
| 24 | MBI | Mabian | 139.5 | 2.0 | 0.73 | 0.05 | 12 | 1 |
| 25 | MDS | Mendingshan | 173.9 | 10.8 | 0.71 | 0.26 | 9 | 1 |
| 26 | MEK | Maerkang | 144. 4 | 6.9 | 0.89 | 0.10 | 11 | 1 |
| 27 | MGU | Meigu | 152.2 | 8.6 | 0.67 | 0.08 | 7 | 1 |
| 28 | MLI | Muli | 175.7 | 21.4 | 0.88 | 0.37 | 5 | 1 |
| 29 | MNI | Mianning | 173.7 | 5.4 | 0.75 | 0.08 | 10 | 1 |
| 30 | MXI | Maoxian | 101.6 | 6.9 | 0.66 | 0.18 | 3 | 1 |
| 31 | PGE | Puge | 1.7 | 5.3 | 0.67 | 0.05 | 15 | 1 |
| 32 | PWU | Pingwu | 112.1 | 5.1 | 0.88 | 0.11 | 13 | 1 |
| 33 | QCH | Qingchuan | 43 | 3.7 | 1.01 | 0.13 | 11 | 1 |
| 34 | REG | Ruoergai | 123.5 | 2.3 | 1.43 | 0.11 | 14 | 1 |
| 35 | RTA | Rangtang | 155.1 | 6 | 1.16 | 0.07 | 18 | 1 |
| 36 | SMI | Shimian | 109.9 | 2.0 | 0.90 | 0.13 | 11 | 1 |
| 37 | SMK | Shimenkan | 132.8 | 9.9 | 0.79 | 0.32 | 7 | 1 |
| 38 | SPA | Songpan | 72.3 | 5.8 | 0.88 | 0.15 | 10 | 1 |
| 39 | WCH | Wenchuan | 11.6 | 10.8 | 0.86 | 0.42 | 6 | 1 |
| 40 | WMP | Wumaping | 131.3 | 2.5 | 0.87 | 0.05 | 11 | 1 |
| 41 | XCH | Xiangcheng | 2.0 | 5.9 | 0.94 | 0.12 | 11 | 1 |
| 42 | XCO | Xichong | 100.9 | 2.8 | 0.59 | 0.07 | 12 | 1 |
| 43 | XHA | Xuanhan | 109.8 | 4.7 | 0.65 | 0.08 | 14 | 1 |
| 44 | XJI | Xiaojin | 141.7 | 4.5 | 0.65 | 0.12 | 8 | 1 |
| 45 | XJP | Xianjiaping | 168.5 | 4.5 | 0.50 | 0.01 | 12 | 1 |
| 46 | XSB | Xuanshengba | 162.4 | 8.3 | 0.78 | 0.06 | 9 | 1 |
| 47 | YGD | Youguanding | 121.5 | 9.3 | 1.08 | 0.21 | 6 | 1 |

| | | | | | | | | |
|----|------|-------------|-------|------|------|------|----|---|
| 48 | YJI | Yajiang | 86.2 | 3.2 | 1.38 | 0.10 | 17 | 1 |
| 49 | YYC | Yuanyichang | 140.1 | 5.5 | 0.92 | 0.11 | 8 | 1 |
| 50 | YYU | Yanyuan | 129.2 | 4.9 | 0.63 | 0.12 | 9 | 1 |
| 51 | YZP | Youzhaping | 2.9 | 19.3 | 0.64 | 0.10 | 3 | 1 |
| 52 | ZJG | Zhongjiagou | 119.9 | 3.5 | 1.36 | 0.14 | 3 | 1 |
| 53 | CHX | Chengxian | 115.9 | 1.8 | 1.03 | 0.13 | 9 | 2 |
| 54 | DBU | Diebu | 114.5 | 3.1 | 1.16 | 0.13 | 16 | 2 |
| 55 | MIX | Minxian | 119.7 | 3.4 | 0.70 | 0.13 | 3 | 2 |
| 56 | MAQI | Maqinquin | 131.8 | 3.0 | 0.82 | 0.10 | 4 | 2 |
| 57 | MQU | Maqu | 131.2 | 5.9 | 1.57 | 0.20 | 8 | 2 |
| 58 | TSH | Tianshui | 121.3 | 3.3 | 1.12 | 0.24 | 5 | 2 |
| 59 | WEX | Wenxian | 97.9 | 6.0 | 1.1 | 0.18 | 6 | 2 |
| 60 | WUD | Wudu | 96.5 | 9.4 | 0.83 | 0.14 | 11 | 2 |
| 61 | ZHQ | Zhouqu | 116.1 | 4.4 | 1.24 | 0.24 | 4 | 2 |
| 62 | ANK | Ankang | 107.2 | 4.3 | 0.57 | 0.11 | 7 | 3 |
| 63 | HZH | Hanzhong | 46.6 | 4.4 | 0.70 | 0.13 | 9 | 3 |
| 64 | LUY | Luoyang | 110.3 | 13.5 | 0.83 | 0.16 | 2 | 3 |
| 65 | MAX | Mianxian | 73.1 | 11.4 | 0.50 | 0.08 | 7 | 3 |
| 66 | TAB | Taibai | 105.8 | 3.8 | 0.85 | 0.09 | 13 | 3 |
| 67 | XIX | Xixiang | 60.8 | 9.5 | 0.58 | 0.05 | 11 | 3 |
| 68 | ZOZ | Zhouzhi | 101.2 | 3.6 | 1.23 | 0.10 | 9 | 3 |
| 69 | CHS | Changshou | 141.8 | 7.7 | 0.57 | 0.10 | 5 | 4 |
| 70 | FUL | Fuling | 151.1 | 12.3 | 1.18 | 0.44 | 4 | 4 |
| 71 | ROC | Rongchang | 126.1 | 8.3 | 0.83 | 0.10 | 4 | 4 |
| 72 | SHZ | Shizhu | 169.4 | 6.1 | 0.72 | 0.20 | 4 | 4 |
| 73 | SNB | Nanbin | 100.7 | 2.2 | 0.89 | 0.08 | 7 | 4 |
| 74 | WAZ | Wanliu | 138.4 | 10.6 | 0.82 | 0.25 | 2 | 4 |
| 75 | WRC | Ruichi | 140.8 | 5.6 | 0.47 | 0.11 | 5 | 4 |
| 76 | WUL | Wuling | 132.9 | 20 | 0.65 | 0.39 | 1 | 4 |
| 77 | HEQ | Heqing | 132.1 | 3.3 | 0.76 | 0.10 | 23 | 5 |
| 78 | LIJ | Lijiang | 8.2 | 2.6 | 1.68 | 0.13 | 5 | 5 |
| 79 | YSH | Yongsheng | 175.4 | 5.5 | 0.72 | 0.10 | 16 | 5 |
| 80 | ZHD | Zhongdian | 178.0 | 4.9 | 0.82 | 0.20 | 7 | 5 |
| 81 | ZOT | Zhaotong | 134.2 | 1.9 | 1.08 | 0.11 | 12 | 5 |
| 82 | CD2 | Chengdu | 124.9 | 2.4 | 1.00 | 0.12 | 12 | 6 |

| | | | | | | | | |
|----|-----|------------|-------|------|------|------|----|---|
| 83 | GYA | Guizhou | 160.5 | 6.8 | 0.52 | 0.04 | 18 | 6 |
| 84 | PZH | Panzhihua | 108.7 | 4.9 | 1.18 | 0.21 | 15 | 6 |
| 85 | DGN | Daguan | 142.8 | 6.6 | 0.59 | 0.12 | 4 | 7 |
| 86 | JCH | Jianchuan | 98.0 | 10.0 | 0.88 | 0.20 | 3 | 7 |
| 87 | NLG | Ninglang | 18.0 | 4.6 | 1.35 | 0.08 | 2 | 7 |
| 88 | DAB | Danba | 142.1 | 3.9 | 1.03 | 0.15 | 4 | 8 |
| 89 | DNB | Dengba | 139.7 | 4.6 | 0.53 | 0.21 | 9 | 8 |
| 90 | HLS | Honglashan | 172.7 | 14.4 | 0.87 | 0.16 | 2 | 8 |
| 91 | HNI | Heni | 175.5 | 3.6 | 1.24 | 0.08 | 10 | 8 |
| 92 | LUH | Luhuo | 129.1 | 7.7 | 1.15 | 0.27 | 6 | 8 |
| 93 | MNK | Mangkang | 137.2 | 5.6 | 0.86 | 0.21 | 8 | 8 |
| 94 | YID | Yidun | 5.7 | 3.7 | 0.61 | 0.08 | 6 | 8 |

Where φ is fast-wave direction, $\Delta\varphi$ is the error of the fast-wave direction, δt is delay time, $\Delta\delta t$ is the error of the delay time. Remarks: 1, Sichuan regional digital seismograph network (52 stations from Jan. 2007 to June 2008); 2, Gansu regional digital seismograph network (9 stations from July 2007 to June 2008); 3, Shanxi regional digital seismograph network (7 stations from July 2007 to June 2008); 4, Chongqing regional digital seismograph network (8 stations from July 2007 to June 2008); 5, Yunnan regional digital seismograph network (5 stations from Jan. 2002 to Jun. 2008); 6, China National Digital Seismograph Network (3 stations from Jan. 2003 to Jun. 2008); 7, Sino-US temporary seismic observation in Yunnan (3 stations from Nov. 2000 to Apr. 2002); 8, Sino-US temporary seismic observation in western Sichuan and eastern Tibet (7 stations from July 2004 to Apr. 2006).

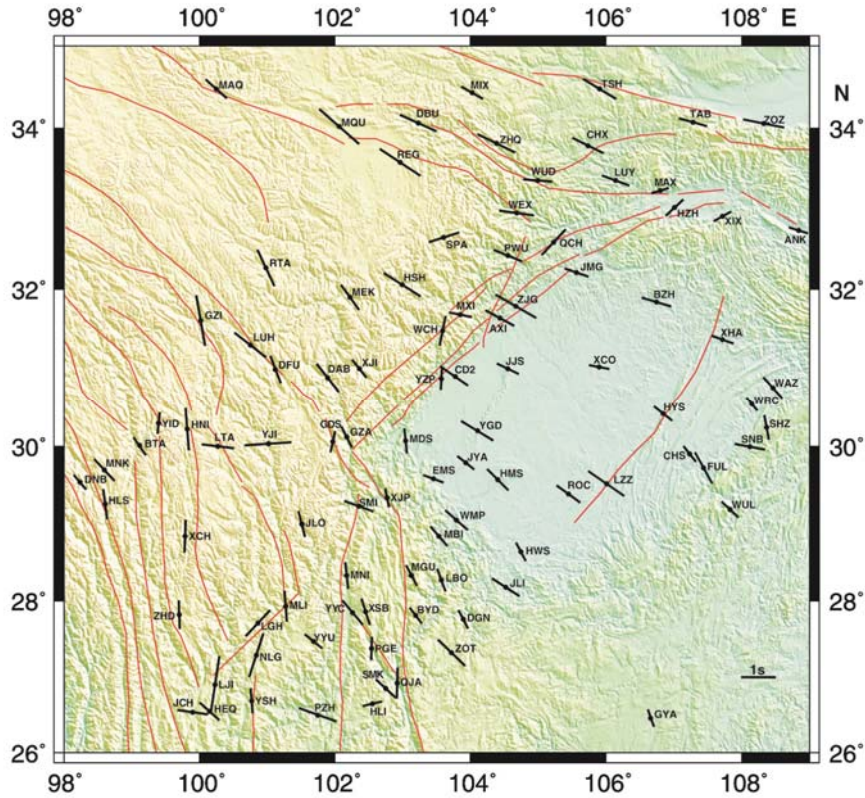


Fig.4 Anisotropic image of upper mantle beneath Sichuan and adjacent regions and regional geologic setting of the study area

The orientations and length of thick line indicate the fast polarization direction and the delay time, respectively. Red lines show major faults.

4. Discussion and Conclusion

4.1 Localization and thickness of anisotropic layer

McNamara et al. (1994)^[10] analyzed the splitting of PS converted wave on the Moho beneath the Tibetan Plateau, and obtained the delay time of 0.17~0.26 s caused by the crustal anisotropy, which is only about 1/5 of the total delay time of SKS splitting (In this study, the delay time between fast and slow waves at most stations is about 1s). The analysis of the contents of olivine and other mineral in upper mantle and laboratory measurement of olivine lattice inferred anisotropy degree of 0.04^[18], in this case, delay time of 1s corresponds to thickness of 115 km. Thus we deduce the anisotropic thickness of upper mantle in the study area is about 54~193 km based on the delay time of 0.47~1.68 s, the average thickness is about 120 km. There exists a large variation of the thickness of anisotropic layer, which implies that the inside lithospheric

deformation is asymmetrical beneath the study area. Other geophysical results show that the structure of the crust and upper mantle exist obviously laterally inhomogeneities^[20-23]. According to the surface wave anisotropy beneath China continent, there exists stronger anisotropy in deep of 70~150 km^[24]. The lithosphere thickness of the Tibetan Plateau is about 160~220 km, and the thickness of the Yangtze block is about 170 km^[25]. Hence, we suggest that the anisotropy in Sichuan and adjacent regions mainly come from upper mantle lithosphere, and the asthenospheric contribution is small.

4.2 Cause of anisotropy

Anisotropy in the upper mantle is a consequence of strain-induced lattice preferred orientation of olivine crystals, it reflect the past and present internal deformation of the subcontinental upper mantle by tectonic episodes. Hence, we can infer kinematic models of the medium of the earth's interior^[17]. For stable continental regions, it is interpreted as “fossil” anisotropy, whereas the anisotropy reflects present-day tectonic activity in tectonic active continental regions.

The strike directions of major faults in the northeastern and western part of the study area are SEE and NS, respectively^[26], where the fast-wave polarization direction is consistent with the strike of the major faults. Comparing with the anisotropy and the velocity field of GPS measurements^[27-29], the fast-wave direction is close to the trends of GPS measurements. These indicate that the deformation models of upper crust and upper mantle are identical, and possibly presence of vertically coherent deformation of crust-mantle in study area. The fast-wave directions of three stations (JCH、PZH and HLI) in the latitude 26.5°N are EW, the fast-wave directions perpendicular to the surface tectonic strike, it could be related to the Burma [back-arc extension](#). Some studies also presented that the geophysical parameters (e.g. crustal thickness, Bouguer gravity anomaly, tectonic stress directions and crust-mantle velocity structure) vary greatly in this zone^[30-33]. The fast-wave directions of EW at stations LIT and YJI in the latitude 30°N can be considered as lithospheric “fossil” anisotropy. The anomaly fast-wave directions at stations QCH、HZH、MAX and MIX in the east segment and at stations YZP and WCH in the west segment of the Longmenshan fault zone are possibly related to the local fault strike. Possible reason is the lateral extrusion of the upper mantle material due to the resistance comes from Yangtze block.

The fast-wave polarization directions of NW-SE in the Yangtze block are consistent with the fast-wave directions at stations in the Songpan-Garze block. The delay time on the east of the Longmenshan fault zone is less than that on the west. This implies that the upper mantle material produces the NW-SE deformation in the Yangtze block, but extent of deformation is less than the Tibetan plateau.

4.3 SKS splitting, mantle deformation field and Wenchuan Ms8.0 earthquake

The Longmenshan thrust nappe belt is the boundary between the Songpan-Garze block and Yangtze block. Lou et al.^[34] have studied the Bouguer gravity anomaly in Sichuan and adjacent regions using wavelet transform, and presented that the crustal density in the Sichuan Basin is higher than the crustal density in the Songpan-Garze block. According to crustal velocity structure, the average crustal velocity in the Sichuan Basin is greater than the average crustal velocity in the Songpan-Garze block^[35]. Therefore, the crust in the Yangtze block (Sichuan Basin) is more rigid than the crust in the Songpan-Garze block. The fast-wave directions in the Songpan-Garze block and Yangtze Block are consistent and NW-SE, it implies the deformation patterns of the upper mantle material in the both areas are identical. In the eastern Tibetan Plateau, the crustal material extrude to east or southeast due to SE traction force of the upper mantle material, the extrusion might be obstructed by the rigid block under the Sichuan Basin. After a long-term accumulation of tectonic strain energy, the accumulative energy suddenly released in Yingxiu town of the Longmenshan region, and Wenchuan Ms8.0 earthquake occurred.

Acknowledgements

This research was supported by the National Natural Science Foundation of China (40334041, 40774037), the Special Project for the Fundamental R&D of Institute of Geophysics, China Earthquake Administration (DQJB06B06) and the Special Program of the Ministry of Science and Technology of China (2006FY110100). The broadband seismic data of Sichuan Digital Seismograph Network in this study was provided by Lv Z Y and Dai S G. The data of the adjacent regional Network of Sichuan was provided by National Digital Seismograph Network Data Backup Center. We are grateful for the help of Paul Silver, Lucy Flesch.

Reference:

- 1 Ren J S. The basic characteristics of the tectonic evolution of the continental lithosphere in China. *Regional Geology of China* (in Chinese), 1991, 2: 289–293
- 2 Molnar P, Tapponnier P. Active tectonics of Tibet. *J Geophys Res*, 1978, 83: 5361–5376
- 3 Royden L H, Burchfiel B C, King R W, et al. Surface deformation and lower crustal flow in eastern Tibet. *Science*, 1997, 276: 788–790
- 4 Ricard Y, Ricards M A, Lithgow-Nertelloni C, et al. A geodynamic model of mantle density heterogeneity. *J Geophys Res*, 1993, 98: 21895–21909
- 5 Lithgow-Nertelloni C, Ricards M A. The dynamics of Cenozoic and Mesozoic plate motions. *Rev Geophys*, 1998, 36: 27–78
- 6 Meissner R, Mooney W D, Artemieva I. Seismic anisotropy andmantle creep in young orogens. *Geophys*, 2002, 149: 1–14
- 7 Gao Y, Zheng S H, Zhou H L. Polarization patterns of fast shear wave in Tangshan region and their variations. *Chinese J Geophys* (in Chinese), 1999, 42(2): 228–232
- 8 Zheng X F, Chen C H, Zhang C H. Study on temporal variations of shear-wave splitting in the Chiayi area,aftershock zone of 1999 Chichi earthquake,Taiwan. *Chinese J Geophys* (in Chinese), 2008, 51(1): 149–157
- 9 Silver P G, Chan W W. Share-wave splitting and subcontinental mantle deformation. *J Geophys Res*, 1991, 96: 16429–16454
- 10 McNamara D, Owens T, Silver P G, et al. Shear-wave anisotropy beneath the Tibetan Plateau. *J Geophys Res*, 1994, 99: 13655–13665
- 11 Einat Lev, Maureen D Long, Rob D van der Hilst. Seismic anisotropy in Eastern Tibet from shear wave splitting reveals changes in lithospheric deformation. *Earth Planet Sc Lett*, 2006, 251: 293–304
- 12 Ding Z F, Zeng R S. Observation and study of shear wave anisotropy in Tibetan Plateau. *Chinese J Geophys (Acta Geophysica Sinica)* (in Chinese), 1996, 39(2):211—219
- 13 Jiang M, Xu Z Q, Hirn A, et al. Teleseimic anisotropy and corresponding features of upper mantle in Tibetan Plateau and its neighboring areas. *Acta Geoscientia Sinica* (in Chinese), 2001,22(2): 111—116
- 14 LÜ Q T, Ma K Y, Jiang M. Sismic anisotropy beneath Southern Tibet. *Acta Seismologica Sinica* (in Chinese), 1996, 18(2): 215—223

- 15 Chang L J, Wang C Y, Ding Z F. A study on SKS splitting beneath the Yunnan region. Chinese J Geophys (in Chinese), 2006, 49: 197—204
- 16 Wang C Y, Chang L J, LÜ Z Y, et al. Seismic anisotropy of upper mantle in eastern Tibetan Plateau and related crust-mantle coupling pattern. Sci China Ser D-Earth Sci, 2007, 37(4): 495—503
- 17 Chang L J, Wang C Y, Ding Z F, et al. Seismic anisotropy of upper mantle in [the northeastern margin of the Tibetan Plateau](#). Chinese J Geophys (in Chinese), 2008, 51(2): 431—438
- 18 Vinnik L P, Farra V, Romanowicz B. Azimuthal anisotropy in the Earth from observations of SKS at Geoscope and NARS broadband stations. Bull Sesimol Soc Am, 1989, 79: 1452—1558
- 19 Wolfe C J, Silver P G. Seismic anisotropy of oceanic upper mantle: Shear wave splitting methodologies and observations. J Geophys Res, 1998, 103(B1): 749—771
- 20 Wang C Y, Chan W W, Mooney W D. 3-D velocity structure of crust and upper mantle in southwestern China and its tectonic implications. J Geophys Res, 2003, 108 (B9), 2442, doi:10.1029/2002JB001973
- 21 Zhang Z J, Bai Z M, Wang C Y, et al. The crustal structure under Sanjiang and its dynamic implications: Revealed by seismic reflection/refraction profiling between Zhefang and Binchuan, Yunnan. Sci China Ser D-Earth Sci, 2005, 48(9): 1329—1336
- 22 Zhang Z J, Bai Z M, Wang C Y, et al. The crustal structure of Gondawana and Yangtze blocks: An example by wide angle seismic reflection profiling between Menglian and Malong. Sci China Ser D-Earth Sci, 2005, 48(11): 1828—1836
- 23 Wang C Y, Lou H, LÜ Z Y, et al. The crustal and upper mantle S wave velocity structure in eastern Tibetan Plateau—the deep tectonic background of low crustal flow. Sci China Ser D-Earth Sci, 2008, 38(1): 22—32
- 24 Peng Y J, Huang Z X, Su W, et al. Anisotropy in crust and upper mantle beneath China continent and its adjacent seas. Chinese J Geophys (in Chinese), 2007, 50(3):752—759
- 25 An M, Shi Y. Lithospheric Thickness of the Chinese Continent. Phys Earth Planet Ints, 2006, 159: 257—266.
- 26 Ding G Y. Lithospheres dynamics of China. Beijing: Seismological Press (in Chinese), 1991
- 27 Gan W J, Shen Z K, Zhang P Z, et al. Horizontal crustal movement of Tibetan from GPS measurements. J Geodesy and Geodynamics (in Chinese), 2004, 24(1): 29—35

- 28 Zhang P Z, Shen Z K, Wang M, et al. Continuous deformation of the Tibetan Plateau from global positioning system data. *Geology*, 2004, 32(9), 809–812
- 29 Chen Z, Burchfiel B C, Liu Y, et al. Global Positioning System measurements from eastern Tibet and their implications for India/Eurasia intercontinental deformation. *J. Geophys. Res.* 2000, (105): 16215–16228
- 30 Teng J W, Zeng R S, Yan Y F, et al. The depth distribution of Moho and tectonic framework in eastern Asian continent and its adjacent ocean areas. *Sci China Ser D-Earth Sci*, 2002, 32(2): 89—100
- 31 Ma X Y. Map of Lithospheric Dynamics in China and the Vicinity. Beijing: Geological Publishing House (in Chinese), 1989
- 32 Xu Z H, Wang S Y, Huang Y R, et al. Directions of mean stress axes in southwestern China deduced from microearthquake data. *Chinese J Geophys* (in Chinese), 1987, 30: 476—486
- 33 Li C, R D van der Hilst, Toks M N, Constraining P-wave velocity variations in the upper mantle beneath Southeast Asia. *Phys Earth Planet Inter*, 2006, 154: 180–195
- 34 Lou H, Wang C Y. Wavelet analysis and interpretation of gravity data in Sichuan-Yunnan region, China. *Acta Seismologica Sinica* (in Chinese), 2003, 27(5): 515–523
- 35 Wang C Y, Han W B, Wu J P. Crustal structure beneath the eastern margin of the Tibetan Plateau and its tectonic implications, *Journal of Geophysical Research*, 112, 2007, B07307, doi:10.1029/2005JB003873

Crustal velocity structures beneath North-China revealed by ambient noise tomography

Lihua Fang[†], Jianping Wu, Zhifeng Ding, and Weilai Wang

Institute of Geophysics, China Earthquake Administration, Beijing 100081, China

Abstract We collected continuous waveform data from January 2007 to February 2008 recorded by 190 broadband and 10 very broadband stations of the North-China Seismic Array. The study region is divided into a grid of $0.25^\circ \times 0.25^\circ$, and group velocity distribution maps between 4 s and 30 s were obtained using ambient noise tomography method. The resolution is estimated to be 20-50 km for most of the study area. From the group velocity maps we inverted a 3-D S-wave velocity model using genetic algorithm with smooth constraint. Crustal features observed in the model include sedimentary basins such as North-China Basin, Yanqing-Huailai basin and Datong Basin. A well defined low velocity zone is observed in the Beijing-Tianjin-Tangshan region at 22-30 km depth range, which maybe related with the upwelling of hot mantle material. The high velocity zone near Datong, Shouzhou and Qingshuuhe at 1-23 km depth reveals stable characteristics of Ordos block. The Taihangshan front fault does not penetrate through the Moho discontinuity along the whole fault, probably penetrates through the Moho discontinuity in some region.

Key words: Seismic noise, Surface wave tomography, velocity structure, Genetic algorithm, North-China

1 Introduction

North-China is one of the most seismic active areas in China. Historical strong earthquakes occurred frequently in this area. More than 200 earthquakes with magnitude greater than 5.0 have occurred in this region since 780 BC, among them 37 events are larger than M=6.0 and 10 events are larger than M=7.0 ([The Earthquake Disaster Prevention Department of China Earthquake Administration, 1995, 1999; China Earthquake Networks Center, 2008](#)). In 1679, an earthquake of M= 8.0 occurred in Sanhe, which is the largest one among the known historical earthquakes in this region. The 1976 Tangshan earthquake (M=7.8) killed at least 240,000 people, and was one of the most destructive earthquakes in the world in human history. A detailed investigation of the crustal structure and seismotectonics of this region is very important for the understanding of physics of

* Received 10 May 2010.

† Corresponding author. E-mail: flh@cea-igp.ac.cn

continental earthquakes and for the assessment of seismic hazard and for the mitigation of the seismic risk.

The study region is located at the eastern margin of North-China (Figure 1a). The central part of the study area is North China Basin (NCB). NCB is a large epicontinental basin where many uplifts and depression basins developed since the Cenozoic. NCB can be divided into two major internal uplifts (Chengning, Cangxian) and four major depressions (Jizhong, Huanghua, Jiyang, and Linqing) (Chang, 1991). The northeastern part of the study area is occupied by the relatively stable Yanshan uplift with its major structure and tectonic trend oriented in the E-W direction. The western and northwestern portions are dominated by the Taihangshan uplift region with some small intermountain basins. To the southeast there is the Luxi Uplift, and to the east the Bohai Bay. In the NCB and the Taihangshan uplift region there are many active faults oriented in the NE-SW direction. In the two regions, most of the structures and mountain ranges have trends oriented in the NE-SW direction.

(a)

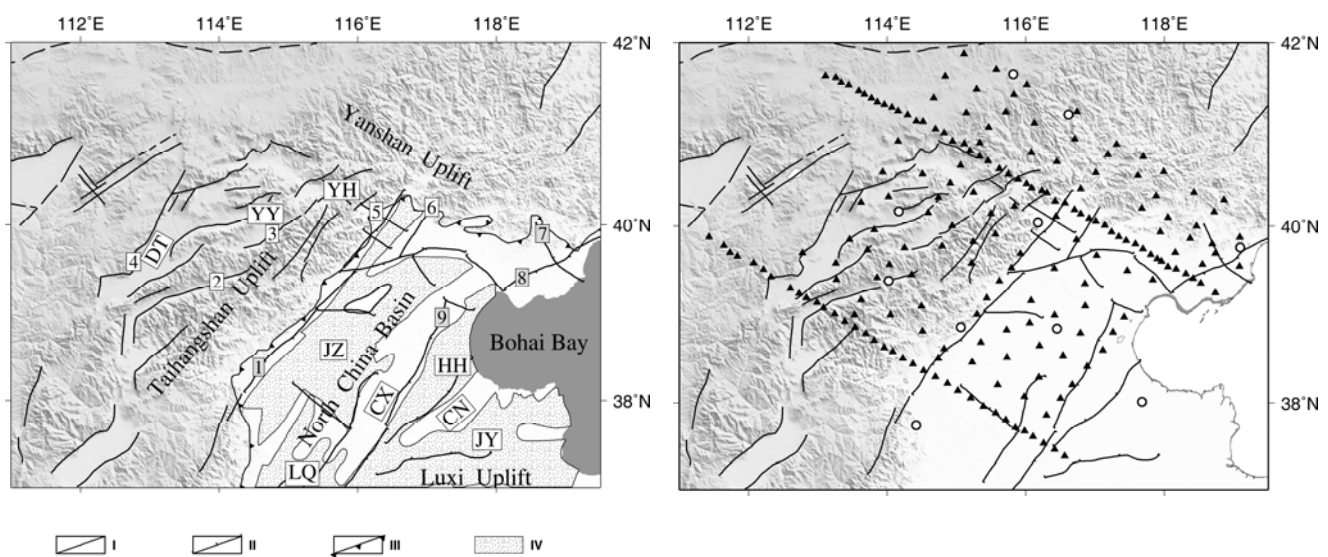


Figure 1 (a) Topography and tectonic sketch map of the study region. Modified from Wang et al.(1989) and Deng et al.(2004). The legend is shown at the bottom. I, Major faults; II, Dduced faults; III, Boundary of Cenozoic basins; IV, Depression areas in North China basin. The names of major faults and geological units are as following: 1, Taihangshan fault; 2, Wutaishan fault; 3, Yuxian-Yanqing fault; 4, Kouquan fault; 5, Nankou-Sunhe fault; 6, Xiadian-Fengheyi fault; 7, Luanxian-Leting fault; 8, Changli-Ninghe fault; 9, Cangxian fault. The names of the basin and major geological units are: YH, Yanqing-Huailai Basin; YY, Yangyuan-Yuxian Basin; DT, Datong Basin; JZ, Jizhong depression; HH, Huanghua depression; JY, Jiyang depression; LQ, Linqing depression; CX, Cangxian uplift; CN, Chengning uplift. **(b)** Locations of the seismic stations used in this study: triangles and circles show the locations of broadband and very broadband stations, respectively.

Extensive geophysical investigations have been conducted in the NCC using the seismic reflection and refraction experiments (Li et al, 2006) and body wave tomography methods (Huang & Zhao, 2004; Qi et al, 2006; Lei et al, 2008). However, these previous results are mainly concentrated on P-wave velocity structures. The receiver function method has been applied to study the S-wave velocity structures (Zheng et al, 2005; Wang et al, 2009). However, the receiver function inversion can only give the velocity structures directly beneath the stations. Many surface

wave tomography studies have also been conducted (e.g., Feng & Teng, 1983; Ritzwoller & Levshin, 1998, Huang et al, 2003), but most of them are at China mainland scale and the lateral resolution is in the order of several to a few hundred kilometers. Few studies of surface waves in North-China have been undertaken, which is due to the relatively low level of seismicity and the consequent logistic limitation suffered by earthquake-based surface wave tomography. Previous studies almost exclusively used teleseismic earthquakes. It is difficult to obtain reliable short-period (<10 s) dispersion measurements from distant earthquakes due to intrinsic attenuation and scattering along the ray paths, and it is these short-period waves that are most useful for constraining the structure of the crust and uppermost mantle. Moreover, the long paths also result in broad lateral sensitivity kernels which limit resolution to hundreds of kilometers. For these reasons, high-resolution surface wave tomography results are scarce in North-China.

Recent studies have shown that the ambient noise tomography method is a powerful tool to image velocity structures beneath dense seismic arrays. This method has been successfully applied in several geographical settings, such as Southern California (Shapiro et al, 2005; Sabra et al, 2005), Tibet (Yao et al, 2006), Europe (Yang et al, 2007), New Zealand (Lin et al, 2007), China (Zheng et al, 2008; Li et al, 2009; Fang et al, 2010, hereafter referred as Paper I), and elsewhere in the world.

In this paper, we present the tomography model of the crust and uppermost mantle beneath North-China, with special emphasis on crustal velocity structures and their implication for our understanding of the present-day seismotectonic setting of the region and the dynamic evolution of North-China. The vertical extent of the model is from the surface to about 50 km depth. We believe that this model will be useful to aid receiver function studies and provide a starting model for other investigations in North-China.

2 Data and Method

A seismic experiment (North China Seismic Array) has been carried out since the winter of 2006. 250 portable stations were deployed in North-China, of which 190 are broadband stations, 10 are very broadband stations and 50 are short period stations. Each station is equipped with Reftek-130B digitizer. The average station separation is about 35 km. Continuous vertical-component seismograms, spanning the period from January 1, 2007 to February 28, 2008 recorded by 190 broadband stations (Guralp CG-3ESPC sensor, 60s to 50Hz flat velocity response) and 10 very broadband stations (Guralp CMG-3T sensor, 120s to 50Hz flat velocity response), are used in this study (Figure 1b).

The data processing procedure that is applied here is described in detail in Paper I. Here we summarize it briefly. Data are processed one day at a time for each station after being decimated to 1 Hz, bandpass filtered in the period band from 4 to 100 s and after the daily trend, the mean and the instrument response are removed. Then the data are normalized by the running-absolute-mean method. The last step of pre-processing is to whiten the data over the

frequency-band of interest. Then the day-long waveform at each station is correlated with that at each of the other stations and the daily results are stacked to produce the final cross correlation. To simplify data analysis and enhance the SNR, we average the positive and negative lags of the cross correlation to form ‘symmetric signals’. The following analysis is done on the symmetric signals exclusively. [Figure 2](#) shows an example of 14-month stacks of cross correlations plotted as a record-section. Clear signals are seen for both positive and negative correlation lags with physically reasonable moveouts ($\sim 3 \text{ km}\cdot\text{s}^{-1}$) of surface waves propagation.

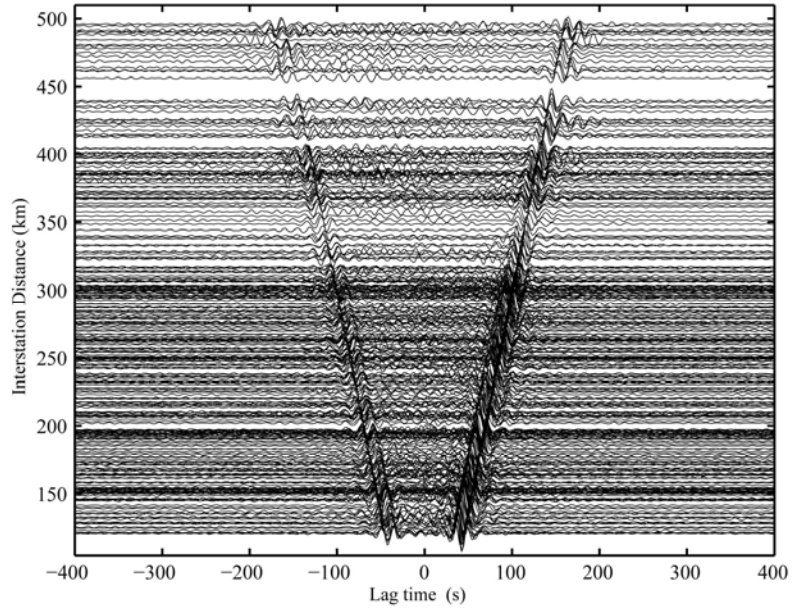


Figure 2 Bandpass filtered (10-50s) cross correlations as a function of distance and lag time. The cross correlation is time reversed if the amplitude of the negative component is smaller than the amplitude of the positive one. Only cross correlation with SNR greater than 25 are plotted.

Rayleigh wave group velocity dispersion curves are determined using a multiple filter method ([Dziewonski et al., 1969](#)). After data selection, 5630 dispersion curves are used to construct the group velocity maps.

3 Group velocity maps

A generalized 2-D linear inversion procedure developed by [Ditmar & Yanovskaya \(1987\)](#) and [Yanovskaya & Ditmar \(1990\)](#) has been applied to construct the group velocity tomographic maps. [Figure 3](#) and [Figure 4](#) show raypath distribution maps and tomography maps for 4.5 s and 20 s, respectively. The lateral resolution is estimated to be 20-50 km.

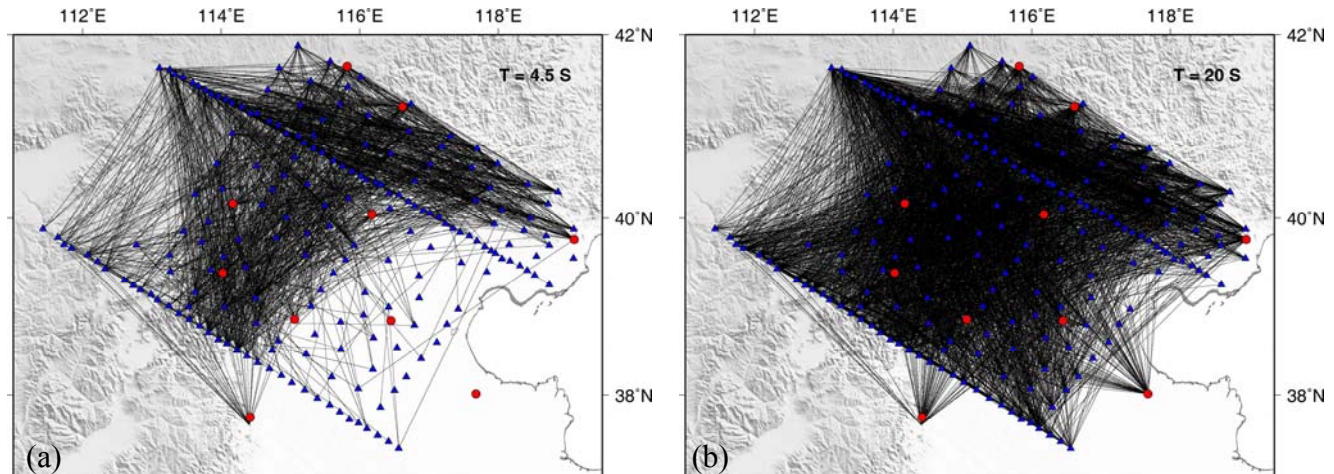


Figure 3 Interstation ray path distribution for group velocity measurements for different periods (4.5 s and 20 s). The broadband stations are shown as blue triangles, while the very broadband stations are shown as red dots.

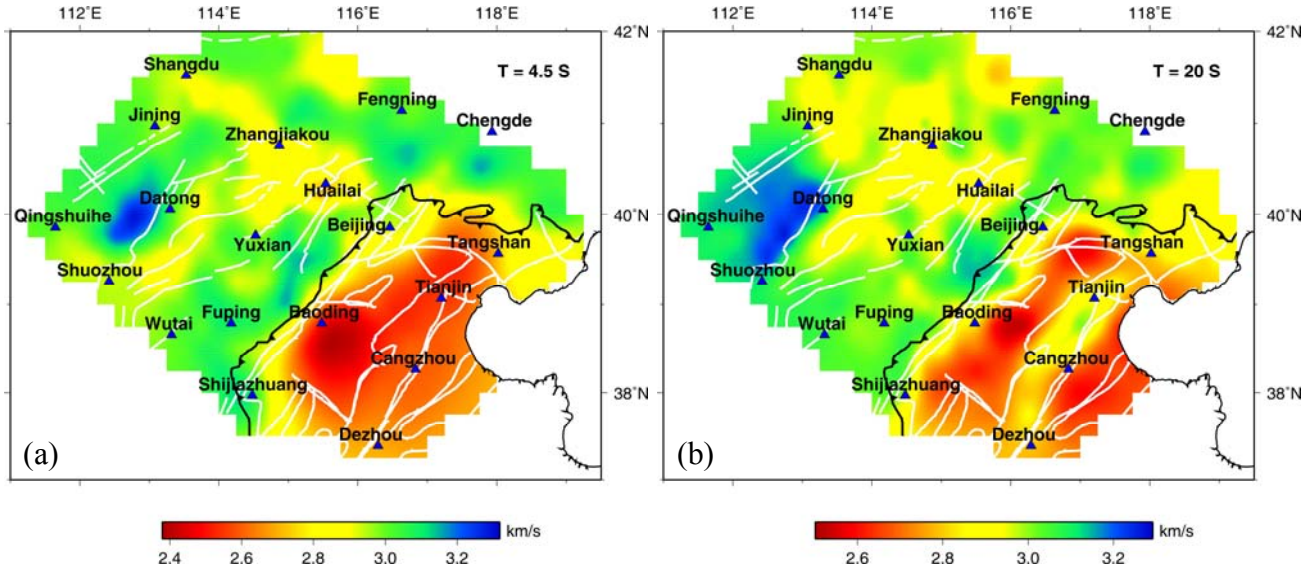


Figure 4 Group velocity maps for different periods (4.5 s and 20 s). The cities are shown as blue triangles.

Due to the length of the paper, we focus on the inversion and interpretation of S-wave velocity structures at different depths. The detailed tomography results are given in Paper I.

4 Structure inversion using genetic algorithm (GA)

4.1 GA optimization

The most important parameters affecting Rayleigh wave propagation are S-wave velocity and layer thickness. Two schemes are often used in inverting dispersion curves. The first way is to fix the layer thickness and only invert S wave velocity. When using this method, the layers are divided as thin as possible in order to adopt model velocity variations and jumps at interfaces. The second way is to invert layer thickness and S wave velocity simultaneously. In general, the first way will increase the uncertainty of inversion results, and rapid oscillations of the solutions are often observed. The second approach can reduce the total number of layers. However, in practice, we do not know the depth of the interface and how many layers should be considered. In addition, the simultaneous inversion of velocity and thickness increases the computing time.

In order to overcome these problems, we use an indirect smooth constraint in GA to invert dispersion curves (Wu et al, 2001). It is very difficult to apply smooth constraint in GA inversion

directly. If the smoothed models are used in iteration, the diversity of models will be greatly suppressed and all models in population tend to be similar with each other after a few iterations. The optimal solution can not be guaranteed. We find that if we do not change the new models generated by selection, crossover and mutation, but modify the model for forward calculation, then the smooth constraint can be easily applied to model parameters in GA inversion.

The process of the method can be summarized as follows: firstly, the new model V_{s0} generated by selection, crossover and mutation is smoothed by equation (1) to produce model V_s , then the smoothed model V_s is used to calculate synthetic dispersion curves. The misfit of model V_{s0} is set to be identical with that of V_s and is used in the next iteration. V_s is only used for the forward calculation, but not in the search of model space. The method is similar to the smooth constraint used in linear inversion.

$$\left\{ \begin{array}{l} V_s(h) = \frac{1}{E} \int_{h-h_0}^{h+h_0} V_{s0}(y) e^{-\sigma(y-h)^2} dy \\ E = \int_{h-h_0}^{h+h_0} e^{-\sigma(y-h)^2} dy \end{array} \right. \quad (1)$$

where V_{s0} is velocity model in GA iteration, V_s is the smoothed model; h_0 is the number of layers used for smoothing. In our case, 3 layers are used for smoothing. However, this value can be adjusted by user. σ is the smooth coefficient. The value of σ depends on the need of model resolution. In general, the smaller σ is, the smoother the model will be. In inversion, σ can be chosen as a function of depth. For example, σ can be selected larger near the surface layer and Moho than in other depth in order to fit the possible large velocity gradients.

After many tests, we find if the layer thickness is thin (less than 3 km), the smooth parameter can be set to 0.2-0.4; if the layer thickness is thick (more than 5 km), the smooth parameter can be set to 0.5-0.7. The smooth parameters also vary with depth. At shallow depth, the smooth parameter can be set to ~ 0.6 . At Moho and other discontinuities, the smooth value can be set to ~ 1.3 .

The key element for any kind of optimization tool is the model evaluation, which is performed by means of an objective function obj that allows a quantitative estimation of the model. We considered the root-mean square value of the difference between the observed and calculated group velocities:

$$obj = \left[\frac{1}{n} \sum_{i=1}^n (v_{obs_i} - v_{cal_i})^2 \right]^{1/2} \quad (2)$$

where n represents the number of observed period-velocity couples, v_{obs_i} is the observed

phase velocity at the i th period and v_{cal_i} is the calculated velocity for the considered model (individual of the current population). This kind of formulation is also referred to as the ℓ_2 -norm.

4.2 Parameterization and priori constraints

Model parameterization strongly affects the inversion results. If the inversion is too weakly constrained, there will be a broad subset of models that will fit the data and large uncertainties will result at each depth. Much tighter constraints on the model space reduce the uncertainty in the estimated parameters, but the model will be increasingly subject to systematic errors.

A priori constraints on the model parameters are important not only to speed the inversion by limiting the volume of model space searched, but also define what we judge to be physically reasonable or plausible candidate models. For these reasons, we collected the seismic reflection and refraction data, receiver function inversion data and receiver function h - k stack results ([China Earthquake Administration, 1986](#); [Zheng et al, 2005](#); [Luo et al, 2008](#); [Xu et al, 2005](#); [Wang et al, 2009](#)).

The depth of Moho is obtained according to Deep Seismic Sounding (DSS) data and receiver function h - k stack results. In inversion, we do not fix the depth of Moho interface, but design a 5-layer model with 1 km thickness near the Moho interface. S-wave velocities near surface (0-4 km) obtained by the receiver function inversion are used to set the search spaces in the uppermost crust. The compressional wave values are calculated using the relation between V_s and V_p ($V_p=1.732*V_s$). When receiver function h - k data are available and the variance is less than 0.05, the ratio of V_p to V_s is set according to RF h - k data. The density is estimated using the Nafe-Drake relation (e.g. [Fowler, 1995](#), [Ludwig et al, 1970](#)). The a priori constraints are applied to ensure that the selected models are physically plausible. A model is considered acceptable if the objective function is less than 0.04.

The period band of dispersion curve used for inversion is 4-30 s. The partial derivatives of the group velocity of Rayleigh wave ([Figure 9, Paper I](#)) shows that the dispersion curve at this period band is sensitive to shear wave velocity structures from surface to 50 km depth, but insensitive to shear wave velocity structures below 150 km. So we construct a starting model with 150 km thickness. The shear wave velocity structures below 150 km are from AK135 model.

[Figure 5](#) shows an example of GA inversion with smooth constraint. The dispersion curve is fit very well. The variations of different models are very small, indicating the inversion approach is feasible and stable.

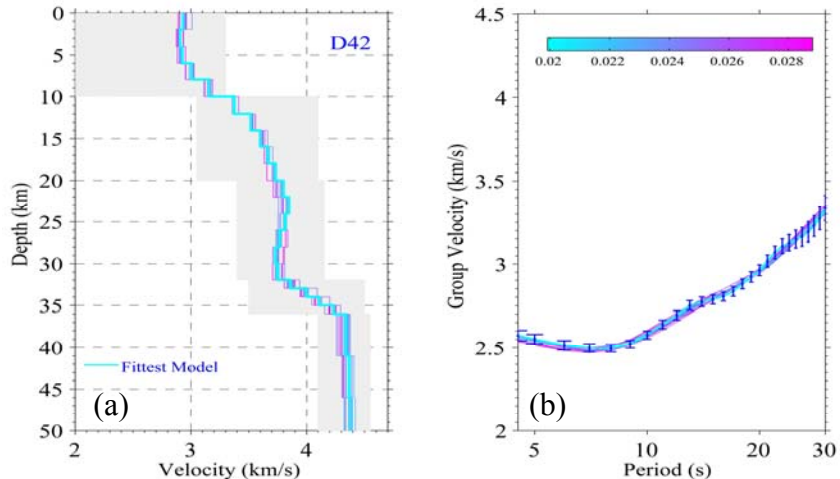


Figure 5 Inversion results of a cell D42. (a) shows S wave velocity structures, (b) shows observed and synthetic dispersion curves. The cyan line in (a) and (b) indicates the best-fit model and dispersion curve, respectively. The gray shaded area in (a) is the search space of S wave velocity in each layer. The color codes in (b) represent misfit values. The error bars in (b) are standard errors of tomography.

5 Crustal and upper-mantle velocity structure

We construct a ‘favoured model’ developed through GA inversion at each gridpoint. Combining these 1-D isotropic models, we obtain a 3-D shear wave velocity model for the North-China, with depth ranging from the surface to about 50 km.

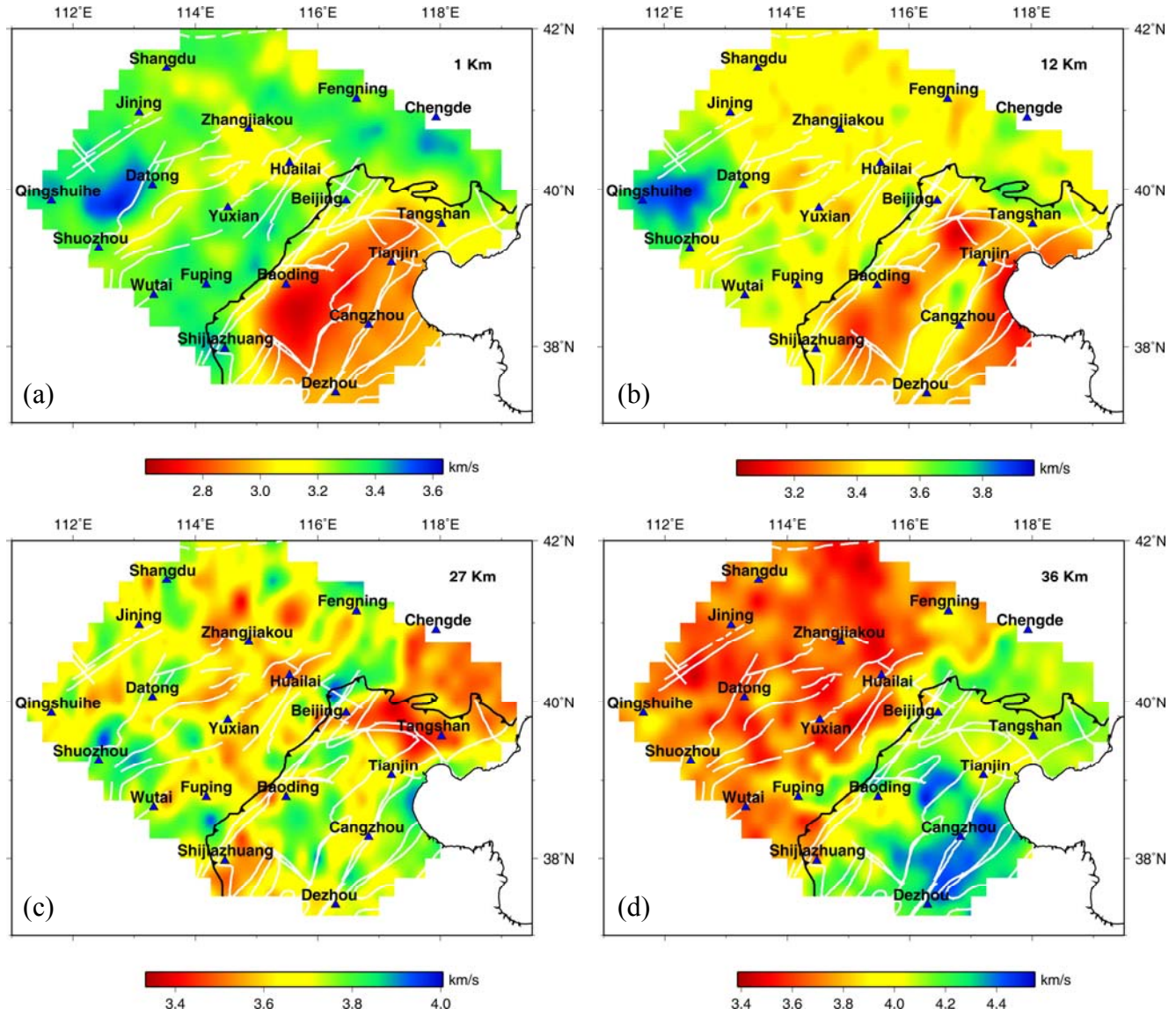


Figure 6 Horizontal slices of S-wave velocities at different depths.

In our study area, the S-wave velocity patterns vary significantly with depth. At 1 km depth ([Figure 6a](#)), the velocity structure is correlated with the sedimentary cover thickness. The boundary between NCB and the surrounding mountain ranges is clearly outlined. A broad low velocity zone is observed at NCB, which is due to the large thickness of sediments. Taihangshan and Yanshan uplifts are imaged as high velocity zones. The Quaternary intermountain basins, such as Yanqing-Huailai, Yangyuan-Yuxian, Datong and Zhangjiakou show up as low-velocity anomalies. In general, the S wave velocity distribution map at 1 km depth correlates very well with known surface geological structures.

At 12 km depth ([Figure 6b](#)), the areas of Jizhong depression, Cangxian Uplift and Huanghua depression are mapped very well. The Jizhong depression and Huanghua depression are mapped with relatively low velocities, while Cangxian uplift is mapped with high velocities. Our results indicate that the sedimentary cover in NCB can reach 10 km thick. The velocity structures clearly reveal that the thickness of sedimentary cover is different in the depression and uplift areas. This is confirmed by DSS and Receiver function inversion study. [Jia & Zhang \(2005\)](#) studied the crust velocity structure of each sub-block in North-China using 30 DSS profiles. Their results reveal that the thicknesses of the sediment deposits in the Huanghua and Jizhong depressions are about 7-9 km and 6-10 km, respectively. [Zheng et al. \(2005\)](#) derived the shear wave velocity model in NCB by inverting the receiver functions obtained at 44 temporary seismic stations. Their results indicate that the sedimentary cover of NCB is about 2-12 km thick.

At 27 km depth ([Figure 6c](#)), a well defined low velocity zone is observed in the Beijing-Tianjin-Tangshan region. This is consistent with many tomography studies in this region. [Zhu & Zeng \(1990\)](#) find a low velocity region in the Beijing-Tianjin-Tangshan region at 50 km depth, which extends to 100 km depth beneath Tangshan and Tianjin. Using regional seismic arrival data and Simultaneous Iterative Reconstruction Technique, [Ding & Zeng \(1994\)](#) reveal that a clear low velocity zone lies between Beijing and Tangshan in the 20-35 km depth range. Recent body wave tomography shows a low velocity zone in the lower crust beneath the Beijing-Tianjin-Tangshan region ([Huang & Zhao, 2004](#)) as well. A high conductivity layer has been found between 20 km to 30 km depth under this region using magnetotelluric soundings ([Liu et al, 1989](#)). In our tomography results, the low velocity zone in the Beijing-Tianjin-Tangshan region can be seen from 22 km to 30 km. We infer that the low velocity zone is related with the upwelling of hot mantle material. Seismic refraction and reflection profiles across Tangshan indicate that there is a 3-5 km offset of Moho discontinuity beneath Tangshan ([Zeng et al, 1988](#)). The hot material of the uppermost mantle may migrate to the crust along the offset of Moho discontinuity. The intrusion of mantle material heats up the lower crust and can cause the reduction of seismic velocity.

At 36 km depth, the velocity slice mainly reflects the velocity structure in lower crust and uppermost mantle in NC ([Figure 6d](#)). Different from the velocity patterns in shallow crust, high velocity anomalies are observed in the eastern part of the study region, while low velocity anomalies are observed in the northwest part. This is because the thickness of crust is different for

the two parts. Reflection and refraction profiles in North-China ([Jia & Zhang, 2005](#)) show that the crust is relatively thin in NCB, while it is thick in the northwest part of our study region: the crust thickness is about 28-29 km in Bohai Bay, about 35-36 km in Beijing and more than 40 km to the west of Taihangshan fault.

From the shear wave velocity slices at different depths, two important features can be seen: (a) a high velocity zone near Datong, Shouzhou and Qingshuihe and (b) strong velocity gradient near the boundary between NCB and Yanshan-Taihangshan uplift. The high velocity zone near Datong, Shouzhou and Qingshuihe is observed at 1-23 km depth. The high velocity zone is located at the northeastern margin of the Ordos block that shares the typical features of cratonic lithosphere and has not been affected by the NCC re-activation. The block is characterized by low seismicity, low heat flow, positive vertical velocity gradient and lack of active fault and magmatic activity ([Qiu et al, 2005](#)). The inversion results reveal the stable characteristics of this region. Strong velocity gradient near the boundary between North-China basin and Yanshan-Taihangshan uplift can be seen at 1-12 km depth. Below 13 km, the high and low velocity anomalies near Taihangshan front fault become blurry, and only can be visible in some parts. We thus argue that the Taihangshan front fault does not penetrate through the Moho discontinuity along the whole fault, probably penetrate through the Moho discontinuity in some region. P-wave tomography has also shown that the Taihangshan front fault cuts through the Moho interface and penetrates into the upper mantle in some parts ([Huang & Zhao, 2004](#), [Zhang et al, 2007](#)).

6 Conclusions

Rayleigh wave empirical Green functions between pairs of stations across North-China are extracted from cross correlations computed using 14 months of ambient noise data recorded from January, 2007 to February, 2008 at 200 temporary stations in North-China. We use dispersion data from Rayleigh wave empirical Green functions to construct high-resolution Raleigh wave group velocity maps in the period band 4-30s. These group velocity maps were then inverted for 3-D shear wave velocity variations in the study region using GA with smooth constraint. The 3-D shear wave velocity model will be useful to aid receiver function studies and provide a starting model for other investigations in North-China.

Crustal features observed in the model include sedimentary basins such as North-China Basin, Yanqing-Huailai basin and Datong Basin. A well defined low velocity zone is observed in the Beijing-Tianjin-Tangshan region at 22-30 km depth range, which maybe related with the upwelling of hot mantle material. The high velocity zone near Datong, Shouzhou and Qingshuihe at 1-23 km depth reveals stable characteristics of Ordos block. The Taihangshan front fault does not penetrate through the Moho discontinuity along the whole fault, probably penetrates through the Moho discontinuity in some region.

Acknowledgments This work is supported by National Natural Science Foundation of China (Grants No. 40774038), the Key Program of the National Natural Science Foundation of China (Grant No. 90914005), Basic Research Project of Ministry of Science & Technology China

(Grants No. 2006FY110100) and National Nonprofit Institute Research Grant of Institute of Geophysics, China Earthquake Administration (Grant No. DQJB09B08).

References

- Chang C (1991). Geological characteristics and distribution patterns of hydrocarbon deposits in the Bohai Bay Basin, east China. *Mar. Pet. Geol.* 8, 98-106.
- China Earthquake Administration (1986). Geophysical exploration results of crust and upper mantle in China. Beijing: Seismological Press.
- China Earthquake Networks Center, Seismic Data Management and Service System (2008). <http://www.csndmc.ac.cn/newweb/index.jsp>.
- Deng Q D, et al. (2004). Distribution of active faults in China (1:4000000). Beijing: Science Press.
- Ding Z F and Zeng R S (1994). The 3D velocity structure inversion in Beijing-Tianjin-Tangshan area by using local earthquake data. *North China Earthquake Sciences*, 12(2), 14-20.
- Dimar P G and Yanovskaya T B (1987). Generalization of Backus-Gilbert method for estimation of lateral variations of surface wave velocities. *Phys. Solid Earth, Izvestia Acad. Sci. U.S.S.R.*, 23 (6), 470-477.
- Dziewonski A M, Bloch S and Ladinsky M (1969). A technique for the analysis of transient seismic signals. *Bull. Seismol. Soc. Am.* 59, 427-444.
- Fang L H, Wu J P, Ding Z F and Panza G F (2010). High resolution Rayleigh wave group velocity tomography in North China from ambient seismic noise, *Geophys. J. Int.* 181, 1171-1182. doi: 10.1111/j.1365-246X.2010.04571.x
- Feng C C and Teng T L (1983). Three-dimensional crust and upper mantle structure of the Eurasian continent, *J. Geophys. Res.*, 88, 2261-2272.
- Fowler C M R (1995). The Solid Earth. An Introduction to Global Geophysics. Cambridge Univ. Press.
- Huang J and Zhao D (2004). Crustal heterogeneity and seismotectonics of the region around Beijing, China, *Tectonophysics*, 385, 159-180.
- Huang Z, Su W, Peng Y, Zheng Y and Li H (2003). Rayleigh wave tomography of China and adjacent regions, *J. Geophys. Res.*, 108(B2), 2073, doi:10.1029/2001JB001696.
- Jia S X and Zhang X K (2005). Crustal structure and comparison of different tectonic blocks in North China. *Chinese J. Geophys. (in Chinese)*, 48(3):611-620.
- Lei J, Xie F, Lan C, Xing C and Ma S (2008). Seismic images under the Beijing region inferred from P and PmP data. *Phys Earth Planet Int.* 168, 134-146.
- Li S L, Mooney W D and Fan J C (2006). Crustal structure of mainland China from deep seismic sounding data, *Tectonophysics*, 420, 239-252.
- Li H., Su W., Wang C. 2009. Ambient noise Rayleigh wave tomography in western Sichuan and eastern Tibet, *Earth Planet. Sci. Lett.* 282, 201-211.
- Lin F C, Ritwoller M H, Townend J, Bannister S and Savage M K (2007). Ambient noise Rayleigh wave tomography of New Zealand. *Geophys. J. Int.*, 170(2), 649-666.
- Liu G, Sun J and Liu J (1989). The electrical structure of the crust and upper mantle in North China. In: Ma, X. (Ed.), *Lithospheric Dynamics Atlas of China*. Beijing: China Cartographic Press, pp. 59-62.
- Ludwig W J, Nafe J E and Drake C L (1970). Seismic refraction. In: *The Sea*, Wiley-Intersci., New York. Vol.4, Part 1:53-84.
- Luo Y, Chong J J, Ni S D, et al. (2008). Moho depth and sedimentary thickness in Capital region, 51(4), 1135-1145.
- Qi C, Zhao D, Chen Y, Chen Q and Wang B (2006). P and S-wave velocity structure and its relationship to strong earthquakes in the Chinese capital region. *Chin. J. Geophys.*, 49 (3), 805-815.
- Qiu R Z, Deng J F, Zhou S, Li J F, Xiao Q H, Wu Z X and Liu C (2005). Lithosphere types in North China: Evidence from geology and geophysics, *Science in China Ser. D Earth Sciences*, Vol.48 No.11 1809-1827.

- Ritzwoller M H and Levshin A L (1998). Eurasian surface wave tomography: Group velocities, *J. Geophys. Res.*, 103, 4839-4878.
- Sabre K G, Gerstoft P, Roux P, Kuperman W A and Fehler M C (2005) Surface wave tomography from microseisms in Southern California, *Geophys. Res. Lett.*, 32, L14311, doi:10.1029/2005GL 023155.
- Shapiro N M, Campillo M, Stehly L and Ritzwoller M H (2005). High resolution surface wave tomography from ambient seismic noise, *Science*, 307, 1615-1618.
- The Earthquake Disaster Prevention Department of China Earthquake Administration (1995). Catalogue of Chinese Historical Strong Earthquakes. Beijing: Seismological Press.
- The Earthquake Disaster Prevention Department of China Earthquake Administration (1999). Catalogue of Chinese Present Earthquakes. Beijing: China Science and Technology Press.
- Wang Y P, Deng Q D and Zhu S L (1989). Lithospheric dynamics of north China. In: Ma, X. (Ed.), *Lithospheric Dynamics Atlas of China*. Beijing: China Cartographic Publishing House, pp:62.
- Wang W L, Wu J P and Fang L H (2009). Crust and upper mantle S-wave velocity structure beneath TangHai-ShangDou seismic array profile. *Chinese J. Geophys. (in Chinese)*, 52(1):81-89.
- Wu J. P., Ming Y. H., Zeng R. S., 2001. Smooth constraint inversion technique in genetic algorithms and its application to surface wave study in the Tibetan Plateau, *Acta Seis,plogical Sinica*, 14, 1, 49-57.
- Xu W W and Zheng T Y (2005). Distribution of Poisson's ratios in the northwestern basin-mountain boundary of the Bohai Bay Basin. *Chinese J. Geophys.(in Chinese)*, 48 (5), 1077-1084.
- Yang Y, Ritzwoller M H, Levshin A L and Shapiro N M (2007). Ambient noise Rayleigh wave tomography across Europe, *Geophys. J. Int.*, 168, 259-274.
- Yanovskaya T B and Ditmar P G (1990). Smoothness criteria in surface wave tomography. *Geophys. J. Int.*, 102:63-72.
- Yao H, van der Hilst R D and de Hoop M V (2006). Surface-wave tomography in SE Tibet from ambient seismic noise and two-station analysis: I.-Phase velocity maps, *Geophys. J. Int.*, 166, 732–744, doi: 10.1111/j.1365–246X.2006.03028.x.
- Zeng R S, Lu H X and Ding Z F (1988). Seismic refraction and reflection profiles across Tangshan epicentral region and their implication to seismogenic processes. *Chinese J. Geophys. (Acta Geophysica Sinica) (in Chinese)*, 31(4), 383-398.
- Zhang L, Liu J S, Hao T Y, Liu J H and Xu Y (2007). Seismic tomography of crust and upper mantle in Bohai Bay baisin and surrounding area, *Science in China Ser. D Earth Sciences*, 37(11), 1444-1455.
- Zheng S, Sun X, Song X, Yang Y and Ritzwoller M H (2008). Surface wave tomography of China from ambient seismic noise correlation, *Geochem. Geophys. Geosyst.*, 9, Q05020, doi:10.1029/2008 GC001981.
- Zheng T, Zhao L and Chen L (2005). A detailed receiver function image of the sedimentary structure in the Bohai Bay Basin, *Phys. Earth Planet. Inter.*, 152, 129-143.
- Zhu L P & Zeng R S (1990). Three-Dimensional P-wave velocity structure under the Beijing network area. *Chinese J. Geophys. (Acta Geophysica Sinica) (in Chinese)*, 33(3), 267-277.

Upper mantle anisotropy beneath the North China from shear-wave splitting measurements

Lijun Chang, Chunyong Wang, Zhifeng Ding

Institute of Geophysics, China Earthquake Administration, Beijing, 100081, China

Abstract

Based on the polarization analysis of teleseismic data, SKS fast-wave directions and delay times between the fast and slow shear waves were determined for each of the 52 seismic stations from both temporary and permanent broadband seismograph networks deployed in the North China Craton (NCC). Both the Silver and Chan and stacking analysis methods were used. In this way, an image of upper mantle anisotropy in the NCC was acquired. The fast-wave polarization directions are basically NWW-SEE in the east, while the fast-wave directions rotate to NNW-SSE in the west. The delay times falls into the interval [0.50 s, 1.39 s]. In the eastern NNC, the fast-wave direction is consistent with the plate motion direction, implying that the NWW trending asthenospheric flow in the upper mantle play a major role in observed anisotropy. The subduction of the Pacific plate has resulted in the asthenospheric mantle flow beneath the eastern NCC, and made the alignment of upper mantle peridotite lattice parallel to the deformation direction, and thus generate consistently NWW trending fast-wave direction. However, shear wave splitting observed in the western NNC was most possibly attributed to the “fossil” anisotropy frozen in continental lithosphere mantle associated with the Precambrian amalgamation between the eastern and western NCC after the closure of ancient oceans.

1. Introduction

Archean cratons are relatively stable tectonic units on the Earth, which are characterized by a cold, thick lithosphere keel. The North China Craton (NCC), however, is an anomaly. In contrast to the long-term stabilization of western NCC, the eastern NCC experienced significant tectonic

rejuvenation (lithospheric thinning of >100km, in particular) in the Mesozoic and Cenozoic. The mechanisms for such a change beneath the NCC is still controversial [Menzies *et al.* 1993; Deng *et al.* 1994; Griffin *et al.*, 1998; Zheng *et al.* 2001]. Some fundamental characteristics are great important to understand the evolution of the NCC, such as the upper mantle deformation beneath the craton and the mantle flow associated with the subduction of the Pacific slab.

The measurement of seismic anisotropy is an effective method for understanding the crust and upper mantle deformation. Researches showed that the upper mantle anisotropy is a consequence of strain-induced lattice preferred orientation (LPO) of olivine crystals [Hess 1964; Nicolas and Christensen, 1987; Savage 1999]. One of the most clear-cut manifestations of anisotropy in seismic data is shear wave splitting. The two splitting parameters, fast-wave direction and the delay time between the fast and slow shear waves, are measures of the orientation and magnitude of mantle deformation, respectively [Silver and Chan, 1991; Liu *et al.*, 2008]. Thus, the researches on anisotropy can be used not only to understand the intraplate deformation features but also to insight the lithospheric or asthenospheric deformation status related to the plate tectonic movements. Previous studies obtained some important results of upper mantle anisotropy in the NCC (Zhao *et al.*, 2005, 2008; Liu *et al.*, 2008; Chang *et al.*, 2008, 2009). However, due to limited data, the understanding of upper mantle anisotropy in the NCC is preliminary. Recently, the seismic array observation in the NCC provides an opportunity to understand further the characteristics of upper mantle deformation.

2. Data and method

The broadband seismic data were recorded at 35 temporary stations in the North China Array observation. Uniformly equipped with REFTEK data loggers and CMG-3ESP sensors (50 Hz-60 s) was operated from October 2006 to March 2009 by Institute of Geophysics, CEA. The NW profile was deployed across the Eastern, Central and Western blocks (see Figure 2). In addition, we collected the data of 17 permanent broadband seismic stations (recorded from July 2007 to November 2009), which come from the regional seismic networks. A total of 53 teleseismic events (Figure 2) were collected at distance between 85° and 110° and with magnitude $M_w > 6.0$ for

shallow earthquake (focal depth<150 km) or $M_w>5.5$ for deep earthquake (focal depth>150 km). Although most events occurred in the southwest Pacific Ocean, several events from other regions have broadened the azimuthal coverage, which improves the resolution of the shear wave splitting parameters.

The SKS splitting analysis in this study involves two steps. Firstly, we used the grid searching method of the minimum transverse energy [Silver and Chan, 1991] to measure the anisotropic parameters and their errors for individual event with different back-azimuths, where 95% confidence is used to the errors estimation. Secondly, a group of anisotropic parameters from all events at a station are stacked by the splitting parameters method [Vinnik et al., 1989; Wolfe and Silver, 1998].

Figure 1 shows an example of SKS splitting analysis, where the distinct transverse component in Figure 1(a) indicates that the SKS wave splits when it propagates through an anisotropic medium. Here the shapes of splitting fast and slow waves are similar in Figure 1(c), and the particle motion is close to elliptic in Figure 1(d). When the splitting effect is removed, the transverse component become negligible in Figure 1(b) and the particle motion is almost linear in Figure 1(f). The minimum energy on the transverse component is well localized on the contour plot as shown in Figure 1(g), which yields the optimum values for the splitting parameters of fast-wave direction and delay time.

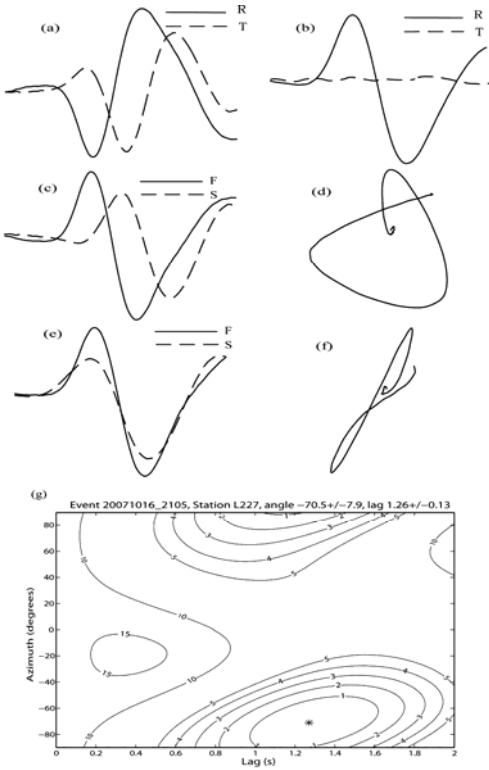


Figure 1. SKS splitting analysis for a teleseismic event (2007/10/16/21/05 with M_w 6.6) at station L227. Original SKS phase (a) and corrected SKS phase (b) in the radial-transverse coordinate system; original SKS phase (c) and particle motion of the original SKS phase (d) in the fast-slow coordinate system; corrected SKS phase (e) and particle motion of the corrected SKS phase (f) in the fast-slow coordinate system; contour plot of energy (g) on the transverse component.

3. Results

The SKS splitting results for 52 stations from the NCC are listed in Table 1 (see auxiliary material). The splitting parameters of 38 of these stations were recently obtained. The results of the rest of the stations have been previously published [Chang et al., 2008, 2009], although we have recalculated the results at some of those stations that have new seismic records. A lot of teleseismic records available for SKS splitting analysis were collected at most stations during the observational period of two and half years. Besides, the involvement of the stacking analysis method enables the measurements with good quality at most stations, in which the errors of fast-wave directions and delay times are less than 10° and 0.2 s, respectively.

Based on polarization analysis from the teleseismic SKS data recorded at the 52 stations in the study area, we developed an anisotropic image of the upper mantle (Figure 2). Figure 2 shows the SKS wave splitting results at 35 temporary stations (black bars) and 17 permanent stations (red bars). The results at temporary and permanent stations are consistent. According to the trend of the observed fast-wave directions, the study area can be divided into two regions as the eastern NCC (the Central and Eastern Blocks) and the western NCC (the Western Block). The average fast-wave directions at stations in the eastern and western NCC are N153°E and N107°E, respectively. The fast-wave directions are basically NWW-SEE in the eastern NCC, while the fast-wave directions rotate to NNW-SSE in the western NCC. The average delay time at 40 stations in eastern NCC is 0.98 s, whereas it is 0.75 s at 12 stations in the western NCC. Thus, the average delay time at stations in the western NCC is less than that in the eastern NCC.

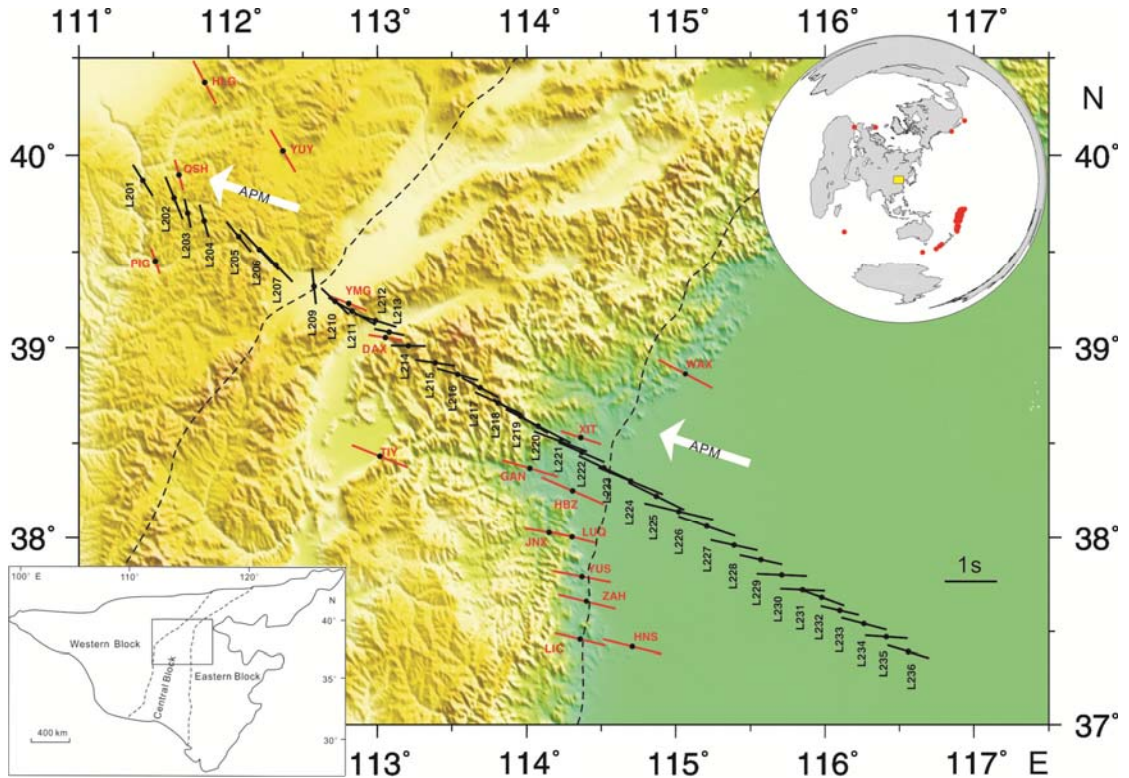


Figure 2. Anisotropic image of upper mantle beneath the NCC. Individual splitting measurements at temporary stations (black bars) and permanent stations (red bars). The orientations and length of bar indicate the fast-wave direction and the delay time, respectively. White arrows represent the APM directions using HS3-NUVEL1a

model (Gripp and Gordon, 2002). The top insert shows the location of the study region (yellow pane) and the distribution of teleseismic events (red circles) used. The bottom inset is a topographic map of the study region showing the threefold division of the NCC; thick dashed lines mark boundaries within the NCC, i.e., the Eastern Block, Central Block and Western Block.

4. Discussion and conclusion

The upper mantle anisotropy is results from the strain-induced LPO of olivine, so that shear wave splitting measurements can provide a direct constraint on the geometry of upper mantle deformation and the upper mantle flow field [Long and Silver, 2008]. On the base of the observation that most fast directions are parallel to the absolute plate motion (APM) of plate, some papers proposed that the origin of the continental anisotropy is caused by present-day mantle flow (Vinnik et al., 1992; Silver, 1996). In the eastern NCC, the NWW (\sim N288°E) APM direction (in a hot spot reference frame) using HS3-NUVEL1a model (Gripp and Gordon, 2002) is almost consistent with the fast-wave directions at most stations (Figure 2 and Figure 3a), which images mantle flow play a significant role in the origin of the upper mantle anisotropy.

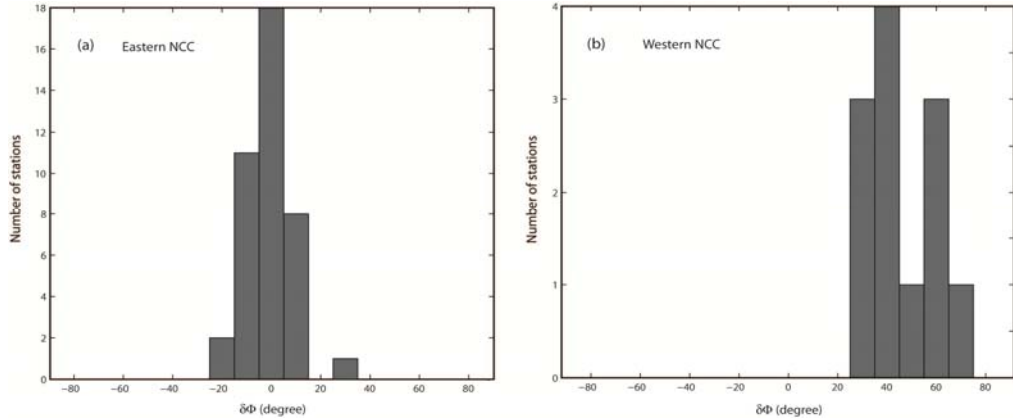


Figure 3. Histograms of difference between the azimuth of the fast-wave direction and the azimuth of APM in the eastern and western NCC are (a) and (b), respectively.

In eastern NCC, the average normalized delay time is 3.53 ms/km in the crust [Wu et al., 2008], the delay time in the crust of 30-40 km thick [Li et al., 2006] is 0.11-0.14 s, which is much less than the average delay time of \sim 1.0 s measured by SKS splitting. Thus, the crustal contribution to SKS splitting is small. For the eastern NCC, overwhelming geochemical and geophysical data

have suggested a thinned lithosphere, with a thickness ranging from 60 to 80 km [Griffin et al., 1998; Huang et al., 2003; Chen et al., 2006], leading to a subcrustal lithosphere thickness of 30-40 km. The average delay time in eastern NCC is ~1 s. This corresponds to a layer of 150 km in thickness with a 3% anisotropy (Liu et al., 2008). Therefore, the lithosphere alone is too thin to produce the observed splitting time, even under the assumption that the crust and the subcrustal lithosphere deform coherently. Hence it is unlikely that lithospheric fabrics contribute significantly to the observed splitting times in the eastern NCC, and consequently, we are left with the options of mantle flow in the asthenosphere.

High-resolution regional tomography studies [e.g., Zhao et al., 2007] revealed that the eastern NCC is in the back-arc region of Japan subduction zone, and is underlain by the Pacific plate. The movement direction of the Pacific plate relative to the Eurasian plate [DeMets et al., 1994] is ~N280°E in the eastern NCC, which is nearly parallel to the NNW trending fast-wave directions. These imply that the NNW trending asthenospheric flow in the upper mantle play a major role in observed anisotropy. The subduction of the Pacific plate has resulted in the asthenospheric mantle flow beneath the eastern NCC, and made the alignment of upper mantle peridotite lattice parallel to the deformation direction, and thus generate consistently NNW-SEE fast-wave direction.

In the western NCC, most splitting at stations in the eastern Ordos Block is weak and thus smaller than the average of 1 s in the eastern NCC, which implies weak intrinsic anisotropy in the stable craton. The NNW-SEE trending fast-wave direction is not only unparallel to the APM direction (Figure 2 and Figure 3b), but also is not consistent with the NE- or NNE regional tectonic trend of surface geological features [Ding, 1991]. The NNW-SEE trending fast-wave direction in the western NCC was most possibly attributed to the “fossil” anisotropy frozen in the continental lithosphere mantle associated with the Precambrian amalgamation between the eastern and western NCC after the closure of ancient oceans. The “fossil” anisotropy can be explained as the result of the deformation of “B-Type” olive fabric under water-rich, high stress and relatively low temperature [Jung and Karato, 2001]. The water-rich collision made the fast-wave direction orthogonal or sub-orthogonal to the striking of the collisional boundary.

Acknowledgments. This research was supported by the National Science Foundation of China (Grant 40904023

and 90914005), the Special Program of the Ministry of Science and Technology of China (Grant 2006FY110100), and the Special Project for the Fundamental R & D of Institute of Geophysics, CEA (Grant DQJB06B06). The data of the permanent stations was provided by Data Management Center of China National Seismic Network at Institute of Geophysics, CEA. We are grateful for the help of Paul Silver, Lucy Flesch, Xu Zhonghuai. We thank two anonymous reviewers for valuable comments and constructive criticism.

References

- Chang, L. J., C. Y. Wang, and Z. F. Ding (2008), SKS splitting beneath Capital area of China, *Acta. Seismol. Sin.*, 21(6), 553-561.
- Chang, L. J., C. Y. Wang, and Z. F. Ding (2009), Seismic anisotropy of upper mantle in eastern China, *Sci. China Ser. D-Earth. Sci.*, 52(6), 774-783.
- Chen, L., T. Y. Zheng, and W. W. Xu (2006), A thinned lithospheric image of the Tanlu Fault Zone, eastern China: constructed from wave equation based receiver function migration, *J. geophys. Res.*, 111, B09312, doi: 10.1029/2005JB003974.
- Deng, J. F., X. X. Mo, H. L. Zhao, Z. H. Luo, and Y. S. Du (1994), Lithosphere root/de-rooting and activation of the East China continent, *Geoscience*, 8(3), 349-356.
- DeMets, C., R.G. Gordon, D. F. Argus, and S. Stein (1994), Effect of recent revisions to the geomagnetic reversal time scale on estimates of current plate motions, *Geophys. Res. Lett.*, 21, 2191-2194.
- Ding, G. Y (1991), Lithospheric Dynamics of China, Beijing: Seismological Press.
- Griffin, W. L., A. Zhang, S. O'Reilly, and C. G. Ryan (1998), Phanerozoic evolution of the lithosphere beneath the Sino-Korean craton, in *Mantle Dynamics and Plate Interactions in East Asia*, *Geophys. Monogr. Ser.*, vol. 27, edited by M. F. J. Flower et al., pp. 107-126, AGU, Washington, D. C.
- Hess, H. H. (1964), Seismic anisotropy of the upper most mantle under oceans, *Nature*, 203, 629-631.
- Huang, Z. X., W. Su, Y. J. Peng, Y. J. Zheng, and H. Y. Li (2003), Rayleigh wave tomography of China and adjacent regions, *J. Geophys. Res.*, 108(B2), 2073, doi: 10.1029/2001JB001696.
- Jung, H., S. Karato (2001), Water-induced fabric transitions in olivine, *Science*, 293, 1460–1463.

Li, S. L., W. D. Mooney, and J. Fan (2006), Crustal structure of mainland China from deep seismic sounding data, *Tectonophysics*, 420, 239-252.

Liu, K. H., S. S. Gao, Y. Gao, and J. Wu (2008), Shear wave splitting and mantle flow associated with the deflected Pacific slab beneath northeast Asia, *J. Geophys. Res.*, 113, B01305, doi: 10.1029/2007JB005178.

Long, M. D., and P. G. Silver (2008), The subduction zone flow field from seismic anisotropy: a global view, *Science*, 319, 315–318.

Menzies, M. A., W. M. Fan, and M. Zhang (1993), Palaeozoic and Cenozoic lithoprobes and the loss of >120 km of Archaean lithosphere, Sino-Korean craton, China, In *Magmatic processes and plate tectonics*, vol. 76, edited by H. M. Prichard et al., pp. 71-78. Geol. Soc. Spel. Pub.

Nicolas, A., and N. I. Christensen (1987), Formation of anisotropy in upper mantle peridotites: A review, in composition structure and dynamics of the lithosphere-asthenosphere system, *Geodyn Ser*, 16, 111-123.

Savage, M. K. (1999), Seismic anisotropy and mantle deformation: What have we learned from shear wave splitting?, *Rev. Geophys.*, 37, 65– 106.

Silver, P. G., and W. W. Chan (1991), Shear wave splitting and subcontinental mantle deformation, *J. Geophys. Res.*, 96, 16,429-16,454.

Silver, P. G. (1996), Seismic anisotropy beneath the continents-probing the depths of geology, *Annu. Rev. Earth Planet. Sci.*, 24, 385–432.

Wu, J., Y. Gao, and Y. T. Chen (2008), Crustal seismic anisotropy in Southeastern Capital area, China, *Acta Seismol Sin*, 21(1), 1-10.

Vinnik, L. P., V. Farra, and B. Romanowicz (1989), Azimuthal anisotropy in the Earth from observations of SKS at Geoscope and NARS broadband stations, *Bull. Sesimol. Soc. Amer.*, 79, 1542-1558.

Vinnik, L. P., L. I. Makeyeva, A. Milev, and A. Yu. Usenko (1992), Global patterns of azimuthal anisotropy and deformations in the continental mantle, *Geophys J Int*, 111: 433-447.

Wolfe, C. J., and P. G. Silver (1998), Seismic anisotropy of oceanic upper mantle: Shear wave splitting methodologies and observations, *J. Geophys. Res.*, 103(B1), 749-771.

Zhao, D., S. Maruyama, and S. Omori (2007), Mantle dynamics of western Pacific and east Asia: Insight from

seismic tomography and mineral physics, *Gondwana Res.*, 11, 120-131.

Zhao, L., and T. Y. Zheng (2005), Using shear wave splitting measurements to investigate the upper mantle anisotropy beneath the North China Craton: distinct variation from east to west, *Geophys. Res. Lett.*, 32, L10309, doi: 10.1029/2005GL022585.

Zhao, L., T. Y. Zheng, G. Lu (2008), Insight into craton evolution: Constraints from shear wave splitting in the North China Craton. *Phys. Earth. Planet. Int.*, 168, 153-162.

Zheng, J. P., S. Y. O'Reill, W. L. Griffin, F. X. Lu, M. Zhang, and N. J. Pearson (2001), Relict refractory mantle beneath the eastern North China block: significance for lithosphere evolution, *Lithos.*, 57, 43-66.